

For Reference

NOT TO BE TAKEN FROM THIS ROOM

For Reference

NOT TO BE TAKEN FROM THIS ROOM

Ex LIBRIS
UNIVERSITATIS
ALBERTAENSIS



1965
#33

THE UNIVERSITY OF ALBERTA

A FEASIBILITY STUDY OF SOLID STATE OPTICAL
DETECTION OF HIGH VELOCITY MICRO-PARTICLES

BY

BRIAN L. CREDICO

A THESIS SUBMITTED TO THE FACULTY OF GRADUATE
STUDIES IN PARTIAL FULFILLMENT OF THE REQUIREMENTS
FOR THE DEGREE OF MASTER OF SCIENCE

DEPARTMENT OF ELECTRICAL ENGINEERING

EDMONTON, ALBERTA

DECEMBER 1965

UNIVERSITY OF ALBERTA

FACULTY OF GRADUATE STUDIES

The undersigned certify that they have read, and recommend to the Faculty of Graduate Studies for acceptance a thesis entitled "Feasibility Study of Solid State Optical Detection of High Velocity Micro-Particles", by Brian L. Credico in partial fulfillment of the requirements for the degree of Master of Science.

ABSTRACT

A method of detecting high velocity micro-particles optically is studied. The particles pass through a narrow beam of light and scatter light into a photomultiplier tube. This thesis studies the feasibility of replacing the photomultiplier with a photodiode and associated solid state electronics. The potential advantages of this method are discussed.

Calculations are made showing it is theoretically possible to detect the micro-particles in the present charging system using a photodiode. A solid state optical detection system is designed and tested. Tests with the micro-particle charger indicate that the amount of useful scattered light received by the solid state optical detector is very much below that calculated. There are indications that very large micro-particles are detected. However, it is concluded that further major changes of the optical detection system are required to provide reliable detection of all sizes of micro-particles of interest.

ACKNOWLEDGEMENTS

The research described in this thesis was carried out at the Department of Electrical Engineering, University of Alberta, under the supervision of E. M. Edwards, to whom the author is indebted for his advice and assistance.

The author would also like to thank F. E. Vermeulen, B. T. Dippie, and the other graduate students for their helpful suggestions and information, and Ed Buck of the machine shop for the proficiency with which he did the necessary machining.

The author is further indebted to the National Research Council and the University of Alberta for financial assistance.

TABLE OF CONTENTS

<u>Section</u>	<u>Page</u>
Introduction	1
1. Signal Light Pulse Characteristics	2
1.1 Pulse Duration	2
1.2 Light Pulse Amplitude	2
1.3 Light Sensitive Device	4
1.4 The Photodiode	7
1.4.1 Sensitivity	7
1.5 Increase of the Apparent Sensitivity of the Photodiode by Means of a Lens System	10
1.6 Biasing of the Photodiode	13
1.6.1 Photodiode Response	13
2. Amplifier Design Requirements	15
2.1.1 Optimum Source Impedance	15
2.1.2 Input Impedance	16
2.1.3 Frequency Response	16
2.1.4 System Gain	18
2.2 Summary of Amplifier Requirements	19
3. Amplifier Electrical Design	20
3.1 Input Stage	20
3.1.1 Input Stage Characteristics	22
3.1.2 Biasing Network	23
3.1.3 Calculation of R_1 and R_2	27

<u>Section</u>	<u>Page</u>
3.2 Second Stage	28
3.2.1 Neutralization of the Gate-Drain Capacity of the Input Stage	31
3.3 Third Stage and Final Circuit Configuration	32
3.4 Summary of the Amplifier Testing	34
3.4.1 Measurement of the Input Shunt Capacity	34
3.4.2 Measurement of the Amplifier Noise Factor	35
4. System Mechanical Design	37
4.1 Mechanical Requirements	37
4.2 System Compatibility	37
4.3 Optical System and Placement	37
4.3.1 Optical Assistance System	40
4.4 Signal to Ground Capacity Shielding	42
5. Summary of System Testing	44
5.1 System Rise Time Measurement	44
5.2 Delay Time Measurement	44
5.3 Displaying of Output Signals	45
5.4 Summary of Testing and Results of the Solid State Optical Detection System When Used with the Micro-Particle Charger	46
Recommendations	49
Bibliography	50
Appendix	52

LIST OF FIGURES

<u>Figure</u>	<u>Page</u>
1-1 Isotropic Light Scattering by a Micro-Particle	3
1-2 Photodiode Characteristic Curve	5
1-3 Equivalent Photodiode Circuit	6
1-4 Measurement of the Photodiode Leakage Current	9
1-6 Collecting Lens	11
1-7 Photodiode Biasing	13
2-1 Response of System to 4 Microsecond Square Light Pulse	16
3-1 Hybrid Compound Source Follower F.E.T.	20
3-2 Biasing Network of the Input Stage	24
3-3 Capacity Voltage Divider Effect of C_1 and C_s	24
3-4 Input to the Amplifier	27
3-5 Bias Voltages	27
3-7 Complimentary Compound Block	29
3-8 Second Stage and Gate-Drain Capacity Neutralization	32
3-9 Complete Amplifier Circuit Diagram	33
3-10 Frequency Response of the Amplifier	34
3-11 Measurement of the Shunt Capacity C_s	35
<u>Photograph</u>	<u>Page</u>
4-1 Disassembled Photodiode Detector	38
4-2 Complete System	39

<u>Figure</u>	<u>Page</u>
4-3 Accessibility to the particle Path	40
4-4 Condenser Lens	41
4-5 Bootstrapped Guarding of the Input	43
5-1 Measurement of the System Delay Time	45
5-2 Method of Displaying the Outputs	46
5-3 Apparatus for Optical Adjustment	46
A-1 Open Loop Equivalent of the Hybrid Compound F.E.T.	52
A-2 Cascaded Amplifiers	52
A-3 Noise Signal To the Amplifier	53

INTRODUCTION

McKinley* has considered meteor phenomena. One particular aspect of the subject is the micrometeoroid. These micrometeoroids are thought to be minute iron particles with a high nickel content and range in size from 0.3 to 300 μ . Due to their extremely small mass micrometeoroids are able to enter the earth's atmosphere without burning up. These micrometeorites are decelerated to their terminal or "free-fall" velocity which is quite slow. It may take up to a month for a micrometeorite to reach the surface of the earth and form what is known as meteoric dust. Various estimates, and data obtained from the Explorer 1 satellite, on the amount of meteoric dust reaching the earth range from a few hundred to 10,000 tons a day. The apparent density of these micrometeoroids in space has led to concern regarding the effect they will have on space vehicles, particularly on extended voyages in space. Since it is difficult to study the effect of micrometeoroid impact while in space, some means of simulating these micrometeoroids in the laboratory is desirable.

* McKinley, D.W.R.: "Meteor Science and Engineering", McGraw Hill, 1961. This book also has a very good bibliography on work related to meteor science and engineering up to 1961.

With this in mind the University of Alberta is in the process of designing an ion dust accelerator which will simulate the micrometeoroids of outer space. At present a micro-particle charger has been constructed in which iron micro-particles of from 2 to 10μ in diameter are brought to velocities of about 0.5 km/sec.

Detection of these particles can presently be accomplished by two methods:

- a) Detection by means of the charge on the micro-particles.
- b) Optical detection, whereby the micro-particle passes through a narrow beam of light and the light so scattered is detected by a photomultiplier tube.

The optical system has the advantage that the micro-particles are still detectable after their charge has been removed.

This thesis is concerned with a study of the feasibility of using a solid state optical detection system consisting of a photodiode and semiconductor electronics in place of the photomultiplier tube.

CHAPTER 1

Signal Light Pulse Characteristics

Before a decision can be made on the adequacy of the photodiode in detecting the microparticles, consideration must be given to the type of light pulse signal expected.

1.1) Pulse Duration

The micro-particle charger will charge small, spherical, iron particles of 2 to 10 microns (1 micron = 10^{-6} m) diameter to a potential of about 20Kv. These particles will be ejected into a 2 mm. diameter light beam at velocities from 0.1 to 0.5 km/sec., the velocity varying inversely as the particle diameter. Assuming that the light beam is uniform, the moving particle will scatter a square light pulse of from 4 to 20 microseconds duration.

1.2) Light Pulse Amplitude

The micro-particles pass through a light beam with an approximate wavelength of 6000°A . Therefore the ratio of particle diameter to the wavelength of the light lies approximately between 3 and 17. Van de Hulst⁽¹⁾ has shown that such micro-particles will scatter incident light almost isotropically.

The light power received at a distance r from the particle is:

$$L_r = \frac{(\text{Area of the intercepting surface}) \times L_o}{\text{Area of the sphere with radius } r}$$

Where L_o = the light power scattered by the micro-particle.

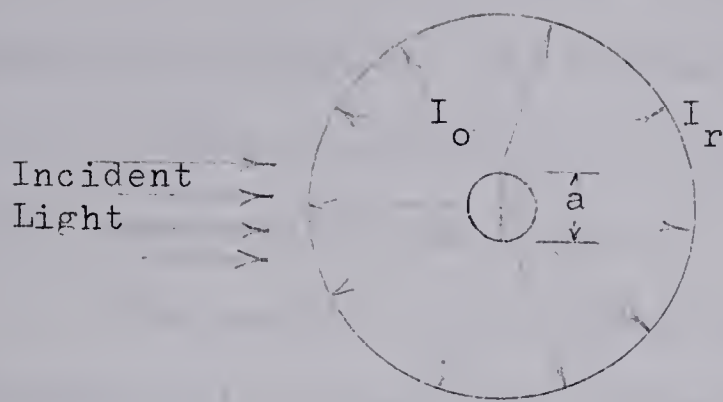


Figure 1-1 Isotropic Light Scattering by a Micro-particle

Referring to figure 1-1, if the diameter of the micro-particle is 'a',

Then:

$$L_r = \frac{(a^2/4)L_o}{4r^2} = \frac{a^2 L_o}{16r^2} \quad (1.1)$$

The ratio of light power scattered by the micro-particle to the light power available in the beam is equal to the ratio of the light intercepting area of the micro-particle to the area of the light beam, assuming perfect reflectivity. This can be expressed as:

$$L_o = \frac{Wa^2}{d_B^2} \quad (1.2)$$

Where:

W = the light power in the beam

d_B = the diameter of the beam

Substituting equation (1.2) into equation (1.1) results in:

$$L_r = \frac{a^4 W}{16d_B^2 r^2} \quad (1.3)$$

For example, if:

$a = 2 \times 10^{-6} \text{ m}$ and the diameter of the light beam is 2mm., then the light power L_r received at a distance $r = 10^{-2} \text{ m}$ from the particle is 0.25×10^{-14} of the available light power incident in the beam.

The present light source available is an arc light which is capable of putting about 100 milliwatts into a 2mm diameter light beam. In the situation above, therefore, the optical detector used must be able to detect a light signal pulse in the order of 0.25×10^{-15} watts.

Factors which will influence the sensitivity of the optical detection system include:

- a) Distance the light sensitive device can be placed from the source of the light pulse signal.
- b) Area of the light collecting surface of the light sensitive device.
- c) Effect of background levels on the operation of the light sensitive device.

1.3 The Light Sensitive Device

The photomultiplier tube presently used to detect the hyper velocity micro-particles has several unsatisfactory features. Among them are high cost, large size and the necessity of a high voltage power supply. The photomultiplier is sensitive to ambient light levels. Ambient light levels will cause a direct current to flow in the dynodes of the

photomultiplier. This results in a different distribution of the dynode potentials. The secondary emitted electrons may no longer be properly focused and the secondary emission coefficient is usually reduced. As a result the sensitivity of the photomultiplier could be severely affected and its linearity reduced.⁽²⁾ Higher ambient light levels would increase the dynode currents to such an extent that the photomultiplier could be damaged. As such, elaborate precautions are necessary to prevent light from the light beam being reflected into the photomultiplier under quiescent conditions.

The photodiode, however, is both extremely small and relatively inexpensive. It requires only low voltages for its operation and, as will be shown below, the photodiode's sensitivity to a pulsed light source is only slightly affected by the ambient light level.

The characteristic curve at a given light input level of a typical photodiode is shown in figure 1-2.

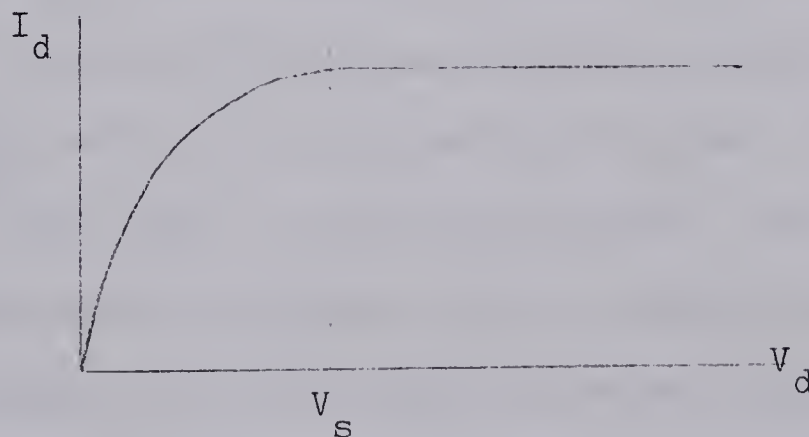


Figure 1-2 Photodiode characteristic curve.

Referring to figures 1-2 and 1-3, at bias voltages above the saturation voltage V_s the photodiode approximates a perfect current source, i.e. it has a very large dynamic resistance of, $\frac{dV_d}{dI_d}$

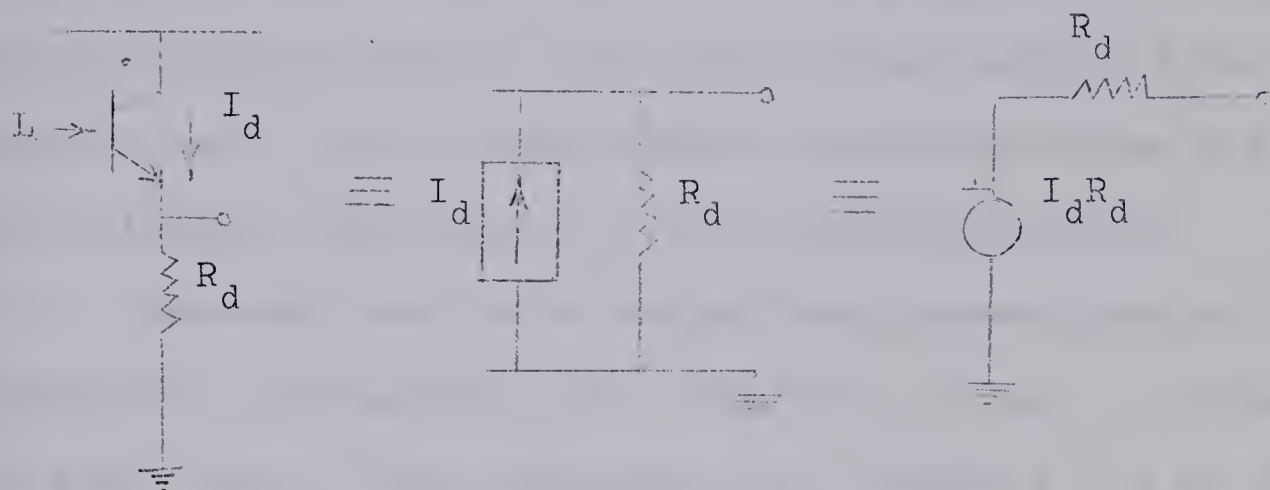


Figure 1-3 Equivalent Photodiode Circuit

As the ambient light level increases the photodiode current I_d , will increase and the voltage drop across the photodiode V_d , will decrease. However, as long as the voltage drop V_d is greater than the saturation voltage V_s the sensitivity, $\frac{dI_d}{dL}$, will be approximately constant, where L is the incident light flux upon the photodiode. Thus the sensitivity of the photodiode to pulsed light is unimpaired as the ambient light increased up to the point where the device saturates.

The upper limit of the ambient light which can be tolerated is the amount of light power required to produce the photodiode saturation current, $I_{ds} = (V_c - V_s)/R_d$.

V_c is the available supply voltage and R_d is the photodiode bias resistor.

For example, if $R_d = 1$ megohm, $V_c = 24$ volts and $V_s = 3$ volts then I_{ds} would be 20 microamps.

A typical photodiode would require about three foot candles of incident light flux to produce this current. Three foot candles is about the light level found outside a few minutes after sunset. This is many orders of magnitude above the tolerable quiescent light level of a photomultiplier tube.

Presently available photodiodes, however, are not as sensitive as photomultipliers. This disadvantage is offset by the small size of the photodiode which enables it to be placed closer to the source of the light signal.

1.4 The Photodiode

The photodiode to be used in the optical detection system should be as sensitive as possible with a low noise level. It should also have a rise time considerably below the expected minimum light pulse duration of 4 microseconds. Investigation of current data sheets resulted in the opinion that the Texas Instrument's LS400 photodiode would be a good choice considering the parameters of sensitivity, noise figure, rise time and cost.

1.4.1 Sensitivity

The rated sensitivity of the LS400 photodiode is 7 microamps/foot candle. Since the area of the photodiode front lens

is $3.55 \times 10^{-6} \text{ m}^2$ the sensitivity of an non-optically assisted LS400 is 114 microamps/microwatt of light flux.

The minimum amount of signal current I_S which can be detected is limited by the noise generated in the photodiode and associated resistors. The noise generated in the photodiode is in the form of shot noise current I_n . Shot noise occurs whenever a current flows and is due to the randomness of the final arrival of the carriers. This randomness gives rise to a uniform frequency spectrum of noise. I_n is related to the direct current in the photodiode by the Schottky equation⁽³⁾.

$$(I_n)^2 = 2q(I_S + I_L)B \quad (1.4)$$

Where:

q = charge on an electron = 1.6×10^{-19} coulomb

I_L = leakage current of the photodiode

$(I_S + I_L)$ = direct current in the photodiode

B = bandwidth of the system $\approx 2 \times 10^6$ cps.

The leakage current of the LS400 photodiode was measured and found to vary linearly with the bias voltage, bias resistor remaining constant. The circuit used for the measurement is shown in figure 1-4. The bias resistor used was the input impedance of the oscilloscope (1 megohm). The leakage current measured with a 1 megohm bias resistor and a 24 volt bias supply V_P , with no light excitation on the photodiode was 100×10^{-12} amps.

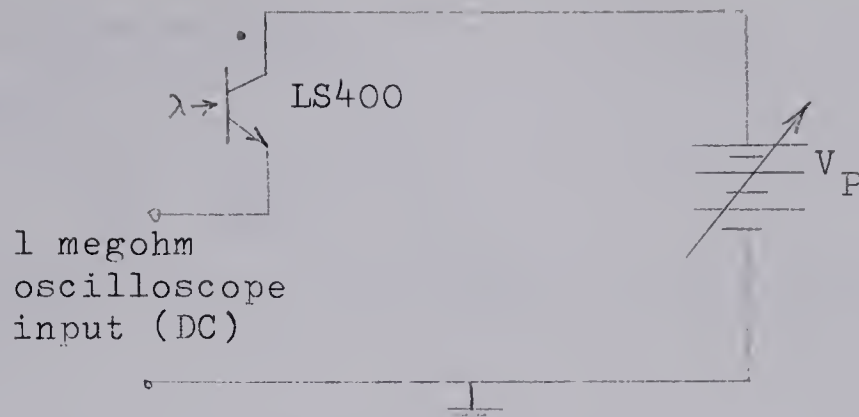


Figure 1-4 Measurement of the Photodiode Leakage Current

The noise voltage e_{ni} which will appear at the input of the amplifier will be the result of the thermal noise voltage generated in R_d and the noise voltage due to the shot noise current of the photodiode through R_c .

Therefore:

$$\overline{e_{ni}^2} = \overline{e_{nR}^2} + \overline{I_n^2 R_d^2}$$

Where:

$$\overline{e_{nR}^2} = 4kTR_d B \quad (1.5)$$

which is the thermal rms noise voltage produced in a resistance⁽⁵⁾.

Where:

k = Boltzmann's constant = 1.374×10^{-23} Joules/ $^{\circ}$ K

T = Temperature in degrees Kelvin

B = Bandwidth of the amplifier

Therefore equation (1.5) may be written as:

$$\overline{e_{ni}^2} = \overline{4kTR_d B} + \overline{2q(I_S + I_L)R_d^2 B} \quad (1.6)$$

It is desired that the signal voltage, e_s be about ten times

the rms noise voltage.

Therefore:

$$e_s = I_s R_d = 10e_{ni}$$

Substituting for e_{ni} in equation 1.6 results in a quadratic in e_s :

$$e_s^2 - 20qe_s R_d B - 10(4kTR_d B + 2qI_L R_d^2 B) = 0$$

For example, assuming a value of $R_d = 1$ megohm and $B = 10^6$ cps, e_s can be calculated from equation (1.8) to be about 1.3 mv rms. Therefore the minimum detectable signal current, I_s , is approximately 1.3×10^{-9} arps.

Since the sensitivity of the photodiode is 114 microamps/microwatt, a light flux of 1.3×10^{-11} watts incident upon the photodiode is needed to produce I_s . The light beam power available at present is not adequate to produce a scattered light pulse of sufficient magnitude such that there will be 1.3×10^{-11} watts incident upon the face of the photodiode. (The available light power is at least 2 orders of magnitude below that required). Some means of increasing the apparent sensitivity of the photodiode is therefore required.

1.5 Increase of the Apparent Sensitivity of the Photodiode by Means of a Lens System

The addition of a lens system effectively increases the light collecting area of the photodiode. This in turn will increase the sensitivity of the system and thus enable a reasonable light beam power to be used.

(11)

If g is the reflectivity of the particle, then from equation (1.2) the light reflected from the particle is now:

$$L_o = \frac{4Wa^2g}{d_B^2} \quad (1.8)$$

It was found in section 1.2 that the light scattered by the micro-particle is isotropic. Assume a collecting lens of diameter d meters is placed outside the light beam a distance x meters from the particle path.

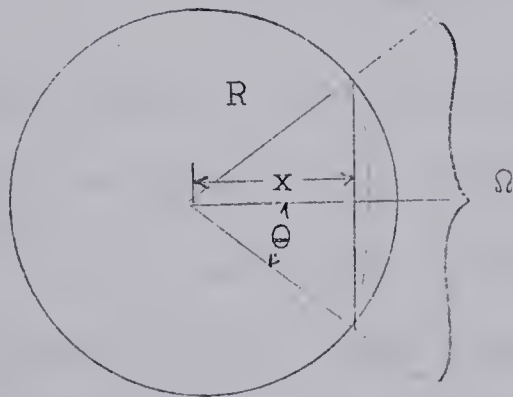


Figure 1-6 Collecting Lens

The total scattered light intercepted by the lens is:

$$L_r = \frac{\Omega L_o}{4\pi} \quad (1.9)$$

Where Ω is the solid angle subtended by the lens and:

$$\Omega = \frac{2\pi R^2 \int_0^L \sin\theta d\theta}{R^2}$$

Where referring to figure 1-6, R is the radius of the sphere

subtended and θ_L is the angle formed between the centerline to the lens and R. $\theta_L = \tan^{-1} \frac{d/2}{x}$

Therefore,:

$$\Omega = 2\pi(1-\cos\theta_L) \quad (1.10)$$

Substituting equations (1.8) and (1.10) into equation (1.9) gives:

$$L_r = \frac{Wa^2g(1-\cos\theta_L)}{2d_B^2} \quad (1.11)$$

Solving for the beam power, W, required:

$$W = \frac{2L_r d_B^2}{a^2 g(1-\cos\theta_L)} \quad (1.12)$$

An approximate value of the beam power required can be found if the parameters of equation (1.12) are estimated as:

$L_r = 1.3 \times 10^{-11}$ watts as found in section 1.4.1

$d_B = 2 \times 10^{-3}$ meters (light beam diameter)

$a = 2 \times 10^{-6}$ meters (micro-particle diameter)

$g = 0.5$ reflectivity factor (assumed)

$\theta_L = \tan^{-1} \frac{d/2}{x}$ where $d = 10^{-2}$ meters (collecting lens diameter)

and $x = 10^{-2}$ meters (distance collecting lens

is from the particle path)

Substituting the above into equation (1.12) results in

$W \cong 0.7$ milliwatts. This light power concentrated in a 2mm

beam can readily be obtained using a concentrated arc light

with a gain by factor of about 10 (the entire

light output is of optimum wavelength for the photodiode.)

The optical system which will be used to assist the photodiode is discussed in section 4.3.1.

1.6 Biasing of the Photodiode

The signal to noise ratio of the photodiode is dependent upon the bias resistor R_d in figure 1-7.

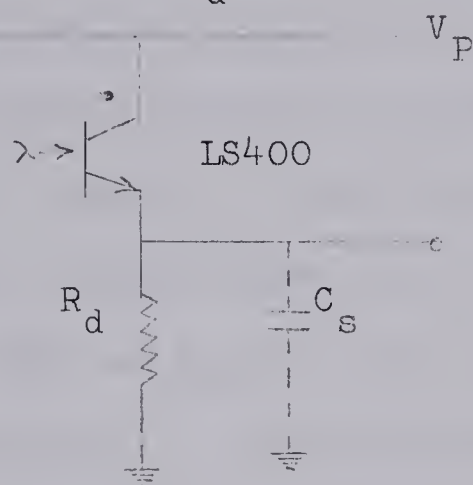


Figure 1-7 Photodiode Biasing

Ideally, for best signal to noise ratio, R_d should be very large. However, as R_d is increased the rise time of the above circuit increases if the stray shunt capacity, C_s , remains constant. This will place an upper limit on R_d .

1.6.1 Photodiode Response

Measurement of the rise time of the LS400 photodiode, connected as in figure 1-7 with $R_d = 2.2K$ and $V_p = 24$ volts, was attempted. The small value of R_d used reduces the effect of any stray shunt capacity to an insignificant factor in determining the rise time of the photodiode. The excitation was provided by a General Radio Strobe-tach which has a one microsecond pulse width of roughly triangular shape and an estimated rise time of from 0.3 to 0.5 microseconds. The rise

time measured at point A in figure 1-7 was 0.5 microseconds. The rise time of the photodiode is therefore less than 0.5 microseconds, exact measurement of which is limited by the experimental apparatus. Thus the rise time of the photodiode will have little effect upon the expected system rise time.

The combination of R_d and the expected stray shunt capacity will largely control the system rise time and as such put a limit upon R_d . It is expected that a system can be designed with a shunt capacity of about 2 pf. This, therefore puts an upper limit on R_d of about 1 megohm if a suitably fast system response is to be obtained. (The required system response is discussed in section 2.1.3.). It was noted previously that R_d should be large for a large signal to noise ratio. Therefore a choice of the maximum value for $R_d = 1$ megohm can be made. This will give an expected signal voltage in the range of at least 10mv.

CHAPTER 2

Amplifier Design Requirements

The design criteria for the amplifier are set by the characteristics of the photodiode and the type of signal which is expected.

2.1.1 Optimum Source Impedance

From section 1.6.1 a value of source resistance, R_d , of the order of 1 megohm was chosen. For a minimum noise figure the optimum source impedance of the amplifier, R_o , should be equal to the source resistance.

For a junction transistor the optimum source impedance can be approximated by: $R_o \cong \sqrt{h_{fe}} h_{ib}$ (19)

This implies that with $R_d = 1$ megohm and $h_{fe} = 100$, h_{ib} must be equal to 100 kilohms. Using the relationship between the transistor collector current I_c and h_{ib}

$$\text{i.e. } h_{ib} = \frac{26 \text{ millivolts}}{I_c} \quad (2.1)$$

the collector current of the junction transistor should be in the order of 300 nanoamps. It would be extremely difficult to operate a junction transistor at this collector current and still maintain an adequately high cut-off frequency.

A solid state device which has an optimum source impedance in the range of 1 megohm at normal operating conditions is the junction field effect transistor. (4)

2.1.2 Input Impedance

At low frequencies the amplifier may be represented as an ideal amplifier with an input impedance R_i . The photodiode, a current source (section 1.3), may also be represented as a voltage generator with the source resistor R_d in series.

The input resistance of the amplifier should be much greater than the bias resistor R_d so it will have a minimal effect upon the operation of the photodiode. If R_i is made very large R_d may be increased, if needed, at a later date with no changes in the amplifier.

A field effect transistor amplifier can be readily designed which will have a low frequency input impedance of $R_i \gg 1$ megohm. The calculated noise figure of such an amplifier will be about 1.04. (Appendix)

2.1.3 Frequency Response

It was observed in section 1.1 that the input light pulses will be 4 to 20 microseconds in duration. The required system rise time can therefore be found assuming that a ten percent signal loss on the 4 microsecond pulse can be tolerated.

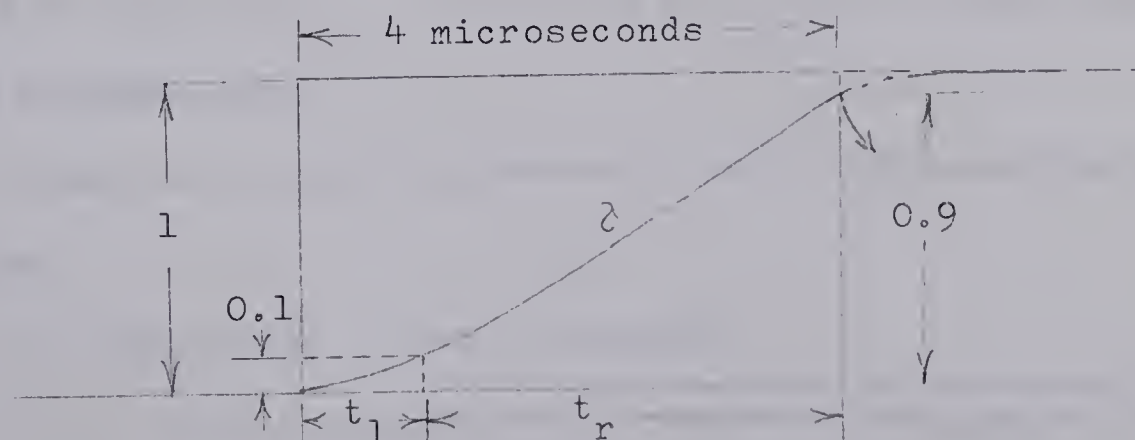


Figure 2.1 Response of system to 4 microsecond square light pulse

The standard exponential response formulae may be applied to the above figure.

$$e_o(t) = E_{SS} \left(1 - e^{-t/\tau} \right) \quad (2.4)$$

Where

$e_o(t)$ = output voltage

E_{SS} = steady state output voltage

t = time in seconds and $\frac{e_o}{E_{SS}} = 0.9$ when

$t = 4 \times 10^{-6}$ seconds (pulse width)

Then the time constant, $\tau = 1.7$ microseconds.

The rise time required of the system is:

$$t_r = t_{\infty} - t_1 \quad (2.5)$$

t_1 is the time required to reach ten percent of the pulse amplitude (figure 2.1), and may be found from formula 2.4

Where:

$$e_o(t) = 0.1 \text{ units}$$

$$E_{SS} = 1.0 \text{ units}$$

$$\tau = 1.7 \text{ microseconds}$$

A value for t_1 of 0.17 microseconds is thus found. Substituting into equation 2.5 results in a required system rise time of 3.83 microseconds.

There are three factors which will influence the system rise time:

1) Rise Time of the Photodiode

The photodiode rise time was investigated in

section 1.6.1 and found to be less than $\frac{1}{2}$ microseconds. It therefore will have insignificant effect upon the system rise time.

2) Voltage Response Rise Time of the Amplifier

The voltage response of the amplifier should have a rise time less than $\frac{1}{2}$ microsecond in order to have minimal affect upon the system rise time. This can be done if the upper corner frequency, f_{3db} , is greater than or equal to 800 kilocycles since $t_r \cong \frac{.35 \text{ to } .45}{f_{3db}}$ (6)

3) RC network formed at the Input of the Amplifier

by the Source Resistance R_d and Stray Shunt Capacity.

This RC network is the most important factor influencing the system rise time. As such, the physical configuration of the input stage and the signal source wiring becomes critical if the stray shunt capacity is to be kept to the necessary minimum. Capacity neutralization will also be necessary.

The low frequency cut-off should be such that there is no more than a 10% droop on the longest expected pulse width of 20 microseconds duration. A lower corner frequency of 600 cps will meet this requirement and is a high enough frequency so as to reduce 60 cps pick-up.

2.1.4 System Gain

At quiescent conditions a noise output level of about

50 mv. peak to peak is desired. This will result in a one centimeter display on a standard oscilloscope running at maximum gain. As such no further amplification, external to the oscilloscope, would be required to detect a signal. The input noise level is assumed to be chiefly the noise voltage generated in the source resistance (section 1.4.1) and an amplifier gain of at least 100 will result in a quiescent noise level output of 10 mv rms.

2.2 Summary of Amplifier Requirements

- 1) Input impedance very much greater than 1 megohm.
- 2) Optimum source impedance approximately equal to 1 megohm.
- 3) Upper corner frequency equal to or greater than 800 kilocycles.
- 4) Amplifier gain greater than or equal to 40 db.

A single ended amplifier, with a hybrid compound F.E.T. in source follower configuration (figure 3-6) as the input stage, can be designed to meet all the above requirements.

CHAPTER 3

Amplifier Electrical Design3.1 Input Stage

The basic circuit of a hybrid compound F.E.T. source follower is shown in figure 3.1.

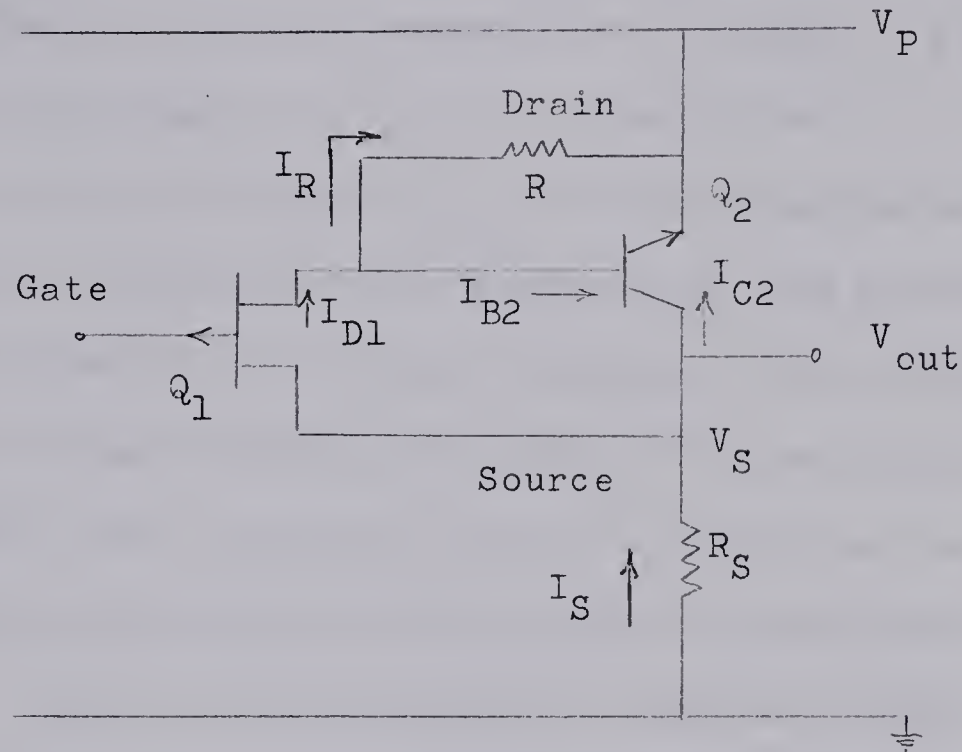


Figure 3.1 Hybrid Compound Source Follower F.E.T.

This compound configuration may be considered as a single field effect transistor with following common source parameters. (18)

$$g'_{is} = g_{is} \quad (3.1)$$

$$g'_{fs} = g_{fs} h_{fe2}^* \quad (3.2)$$

$$g'_{rs} = g_{rs} \quad (3.3)$$

$$g'_{os} = h_{fe2}^* (g_{os} + h_{ob2}) \quad (3.4)$$

Where:

$$h_{fe2}^* = h_{fe2} \frac{R}{R + h_{ib2} h_{fe2}} \quad (3.5)$$

The primed parameters refer to the compound F.E.T.. The subscript "2" refers to the silicon junction transistor Q_2 .

h_{fe2}^* refers to the effective beta.

A F E.T. with good transconductance, bandwidth and noise figure should be used for Q_1 . Q_2 should be a high gain, medium bandwidth junction transistor. Choices of a 2N2606 and 2N3707 were made for Q_1 and Q_2 respectively.

A collector current I_{c2} of one milliampere will enable the 2N3707 to operate at near maximum beta and bandwidth. To maintain a high input impedance the gate of the 2N2606 should not become forward biased with respect to the source. (7)

This implies that the drain current I_D should be less than I_{DSS} (value of the drain current when the gate-source voltage is zero). Q_1 is therefore biased to operate at about 50 microamps drain current which is well below the data sheet specification giving I_{DSS} a value of 170 microamps.

To keep the impedance levels high, the supply voltage V_P should be reasonable high but sufficiently low to prevent breakdown of the semiconductor devices. 24 volts, being readily available and of adequate level, is chosen for V_P .

Measurements on Q_2 showed an h_{fe2} of 400 and a V_{BE2} of 0.63 volts. The base current, I_{B2} , with a one milliampere collector current, is therefore $1/400$ milliampere = 2.5 microamps.

The value of R in figure 3-1 may now be calculated.

$$R = \frac{V_{BE2}}{I_R} = \frac{V_{BE2}}{I_D - I_{B2}}$$

and at the operating currents chosen, $R = 13.3 \text{ K}$. The nearest standard value results in $R = 12 \text{ K}$.

The effective beta of Q_2 may now be calculated from equation (3.5). $h_{fe2}^* = 215$ assuming that $h_{ib2} = 26 \text{ ohms}$ as can be found from equation (2.1).

The gate-source bias point of the F.E.T. which will allow 50 microamps of drain current to flow was found to be $V_{GS} = 0.9 \text{ volts}$ as observed on a curve tracer. This also puts the bias point well into the pinch-off region i.e. the linear portion of the curves, if a source-drain voltage equal to -5 volts is chosen. The pinch-off voltage of the F.E.T. is -2 volts.

R_S in figure 3-1 may now be chosen. If V_S is set equal to -18 volts this will still leave adequate voltage drop across Q_1 and Q_2 and allows a fairly high value of $R_S = 18 \text{ K}$.

3.1.1 Input Stage Characteristics

The measured parameters of Q_1 were taken from the input and output characteristic curves.

$$g_{fs} = 200 \times 10^{-6} \text{ mhos}$$

$$g_{os} = 0.3 \times 10^{-6} \text{ mhos}$$

$$g_{rs} = 2 \times 10^{-12} \text{ mhos}$$

$$g_{is} = 10^{-12} \text{ mhos}$$

The conductance parameters for the hybrid compound F.E.T. are found from equations (3.1) to (3.4).

$$g'_{fs} = 0.052 \text{ mhos}$$

$$g'_{os} = 0.075 \times 10^{-3} \text{ mhos}$$

$$g'_{rs} = 2 \times 10^{-12} \text{ mhos}$$

$$g'_{is} = 10^{-12} \text{ mhos}$$

The source follower input stage characteristics may now be calculated:

The voltage gain is:

$$A_{VS} = \frac{g'_{fs} R_S}{1 + g'_{fs} R_S} = 0.998 \quad (3.6)$$

The output impedance is:

$$Z_{OS} = \frac{1}{g'_{fs}} // R_S = 19.1 \text{ ohms} \quad (3.7)$$

The input impedance is:

$$Z_{IS} = \frac{1}{g'_{is}} = 10^{12} \text{ ohms} \quad (3.8)$$

3.1.2 Biasing Network

The maximum allowable value for R_g , in figure 3-2, is determined from the stability considerations and is calculated from: (8)

$$R_{g(\max)} = \frac{\Delta V_{gs(\max)}}{I_{GSS(\max)}} \quad (3.9)$$

Where:

$I_{GSS(\max)}$ is the leakage current expected in the F.E.T. and may be estimated to be about 5×10^{-11} amps. (10) $\Delta V_{gs(\max)}$

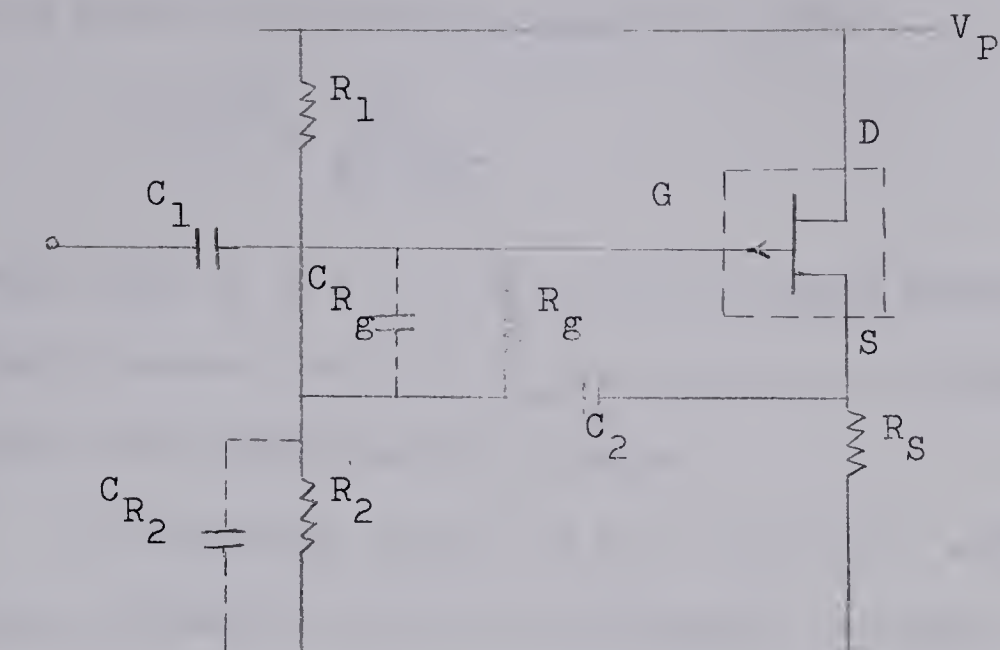


Figure 3-2 Biasing Network of the Input Stage

is the maximum allowable change in V_{GS} so that there will be no greater than a $\pm 25\%$ change in the compound drain current, I_D .

$$\Delta V_{GS} = \frac{\Delta I_D}{g_{fs}} \quad (3.9a)$$

Therefore from equations (3.9) and (3.9a) R_g may be calculated to be 100 megohms.

The capacity voltage divider formed by C_1 and the stray signal to ground capacity C_s could limit the voltage gain available in the input stage. (Figure 3-3) The available

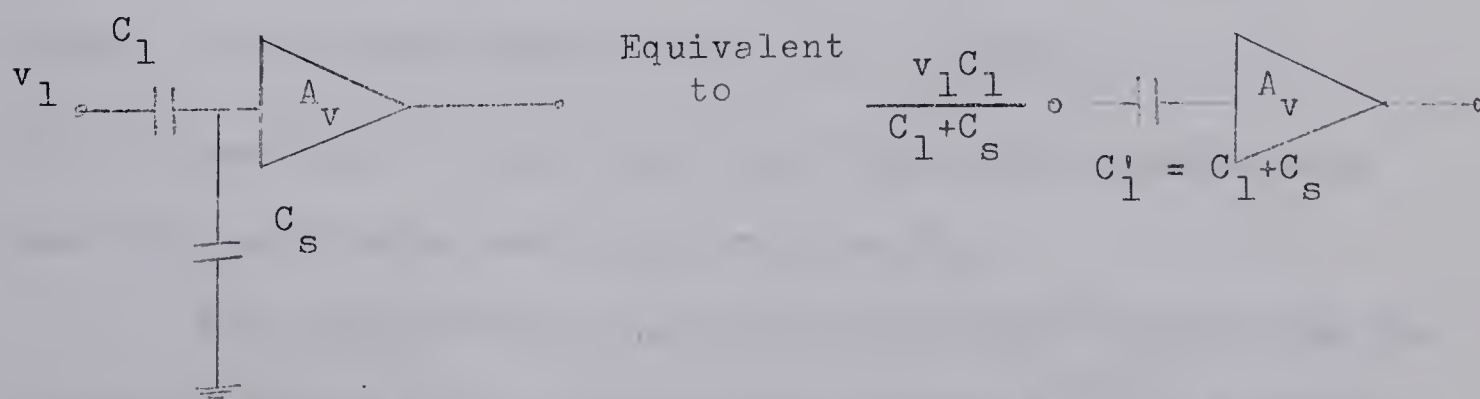


Figure 3-3 Capacity Voltage Divider Effect of C_1 and C_s

voltage gain of the input stage is A'_v where:

$$A'_v = A_v \frac{C_1}{C_1 + C_s}$$

In order that $A'_v \cong A_v$, C_1 must be very much greater than C_s . The low frequency cut-off of the system can be determined by the following amplification stages.

A convenient choice is $C_1 = 0.005$ mf. which results in a gain reduction, due to the capacity voltage divider of only a fraction of one percent.

The source follower configuration of figure 3-2 results in the gate-source capacity, C_{gs} , of the F.E.T. being bootstrapped to an insignificant value of $C_{gs}/(1-A'_{vS})$.⁽¹¹⁾ With the addition of one capacitor, C_2 , the power supply noise is reduced and the shunt capacity C_{R_g} inherent in the resistor R_g is transferred to the output. The circuit so formed in figure 3-2 is now the bootstrapped bias network described by Edwards.⁽¹²⁾

$$\text{Edwards has defined } \alpha = \frac{R_g}{R_C} \quad (3.10)$$

$$\text{where, in this configuration, } R_C = R_g + R_1 // R_2. \quad (3.11)$$

If α is set equal to 0.95 the input stage will require only one very high value and bulky resistor, R_g .

The impedance of C_2 should be very much lower than the impedance formed by R_2 and its shunt capacity C_{R_2} . A value of $C_2 = 1.5C_1 = 0.0075$ mf. will be adequate. Also this ratio

of C_1/C_2 , and the chosen value for α , when applied to the equations derived by Edwards for the bootstrapped bias network result in the following values for the network parameters:

$$\zeta = \zeta_1 = -\gamma = 1 \text{ and } \omega_0 = 7.2 \text{ radians/second}$$

Where:

ζ is the damping factor and the network is critically damped when $\zeta = 1$.

ζ_1 effects the shape of the unit step response. When $\zeta_1 = \zeta$ the initial slope is zero. γ determinis the frequency boost introduced and when γ is negative it introduces a low frequency boost. ω_0 is the characteristic frequency of the network. $\gamma = -1$ and $\zeta = 1$ will result in a low frequency boost of 1.5 db. The peak of the boost will occur at a frequency of 10 radians/second (1.6 cps). Since the following amplifier stages will have a lower corner frequency of about 600 cps, the low frequency boost introduced by the input stage will have no effect upon the system.

The absolute value of the input impedance of figure 3-2 will approach a minimum of $|Z_{in}| = R_g$ at low frequencies. At higher frequencies the input impedance will have an apparent value as high as $|Z_{in}| = R_g/(1-A) \approx 10^{10}$ ohms due to the bootstrapping of R_g .

Thus the addition of C_2 has no detrimental effects on the amplifier when considered with the desired system performance, and does result in some improvement.

The input to the amplifier may be represented as in figure 3-4.

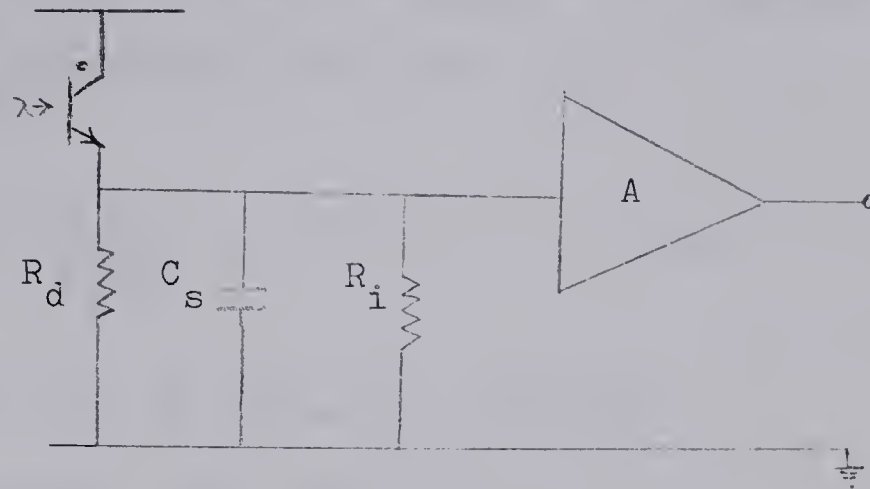


Figure 3-4 Input to the amplifier

C_s is the stray shunt capacity and includes the F.E.T. parallel input capacity and stray input lead wiring capacity.

At high frequencies C_s becomes the dominant term of the input impedance to the amplifier. As discussed in section 2.1.3, C_s in parallel with bias resistor of the photodiode will be the principle factor limiting the rise time of the system.

3.1.3 Calculation of R_1 and R_2

It was found in section 3.1 that a $V_{GS} = 0.9$ volts is needed. This results in a source voltage $V_S = -18$ volts.

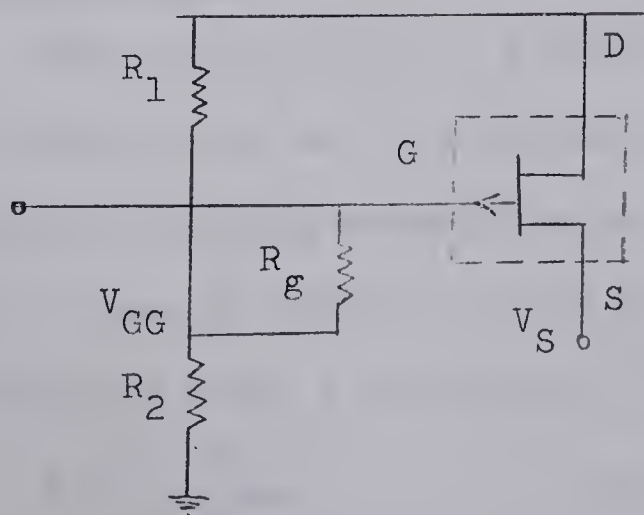


Figure 3-5 Bias Voltages

From figure 3-5, $V_{GG} = V_S - V_{GS} = I_{GSS} R_g$

Using the values found for I_{GSS} and R_g discussed in section 3.1.2 V_{GG} is found to be -17.2 volts.

Also:

$$V_{GG} = \frac{V_P R_2}{R_1 + R_2} \quad (3.12)$$

And where $V_P = 24$ volts, $R_1 = 0.41 R_2$.

From equations (3.10) and (3.11):

$$R_1 // R_2 = \frac{R_1 R_2}{R_1 + R_2} = 5.25 \text{ megohms}$$

And from equation (3.12), $R_1 = 7.5$ megohms and $R_2 = 18$ megohms.

The closest standard value is $R_1 = 8.2$ megohms.

Thus the component values of the input stage, as referred to figure 3-2, are:

$$R_1 = 8.2 \text{ megohms} \quad C_1 = 0.005 \text{ mf}$$

$$R_2 = 18 \text{ megohms} \quad C_2 = 0.0075 \text{ mf}$$

$$R_g = 100 \text{ megohms}$$

$$R_S = 18 \text{ kilohms}$$

3.2 Second Stage

The second stage is a single ended complementary compound connected so as to give the necessary gain bandwidth product combined with a moderately high input impedance. The compound is shown in figure 3-7 and Edwards has shown it to have the following mixed h parameters: (13)

$$h_{ib}^* = \frac{h_{ib1}}{h'_{fe2}} \quad h_{fe}^* = h_{fe1} h'_{fe2}$$

$$h_{ob}^* = h_{ob1} + \frac{h_{ob2}}{h'_{fe2}}$$

$$h_{rb}^* = h_{rb1} + h_{ib1} h_{ob2}$$

Where:

$$h'_{fe2} = \frac{h_{fe2} R}{R + (h_{ib2} + r_d) h_{fe2}}$$

Currents of 120 microamps and 1 milliamp were chosen for Q_1 and Q_2 respectively. At these currents the transistors are operating at near optimum bandwidth with a minimum noise. (13)

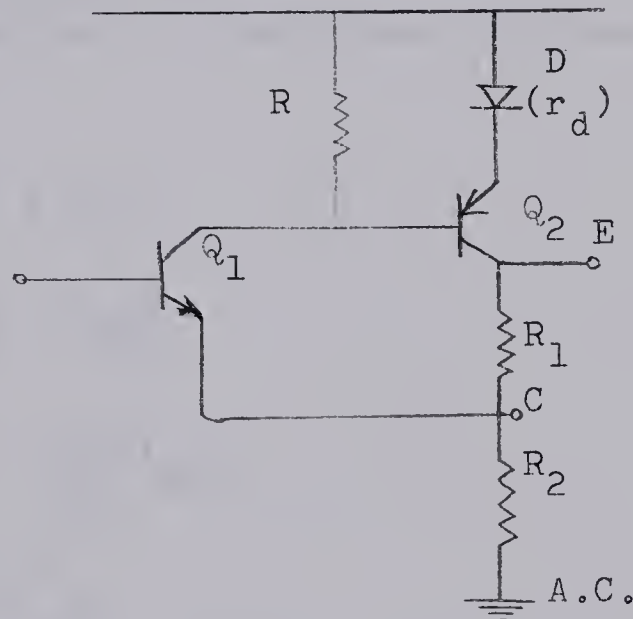


Figure 3-7 Complementary Compound Block

The value of R in figure 3-7, can now be calculated from:

$$R = \frac{V_D + V_{BE2}}{I_{C1} - I_{B2}}$$

Where:

V_D = the voltage drop across the diode D \cong 0.6 volts

V_{BE2} = the base to emitter drop of transistor $Q_2 \cong$ 0.2v

I_{C1} = collector current of transistor Q_1 = 120 microamps.

I_{B2} = base current of Q_2

Therefore $R = 6.8$ kilohms.

With $R_1 = 0$, the circuit is a complementary compound in common collector configuration having load R_2 and voltage gain A_{vC} where:

$$A_{vC} = \frac{1 - h_{rb}^*}{1 + (h_{ib}^*)/R_2} \quad (3.14)$$

and input impedance $Z_{iC} = h_{fe}^* R_2 // \frac{1}{h_{ob2}}$

If $h_{fe2}^* h_{ob2} R_1 \ll 1$, the insertion of R_1 will have negligible effect on the performance of the amplifier as seen from point C.

$$v_E \cong v_C + R_1 i_c^*$$

$$v_E \cong v_C + R_1 \frac{v_C}{R_2}$$

$$v_E \cong (1 + \frac{R_1}{R_2}) A_{vC} v_i$$

$$A_v^* \cong 1 + \frac{R_1}{R_2}$$

The ratio of R_1/R_2 is chosen to give a gain of about 13. The value of R_2 is chosen large enough so that $R_2 \gg h_{ib}^*$. Values of $R_1 = 1.5K$ and $R_2 = 120$ ohms were chosen. The remaining resistive components of the second stage were chosen to give the proper bias points. The capacitors C_3 and C_5 were selected to give a lower corner frequency of about 500 cps and C_6 is added to control the upper frequency response. (Figure 3-8)

3.2.1 Neutralization of the Gate-Drain Capacity of the Input

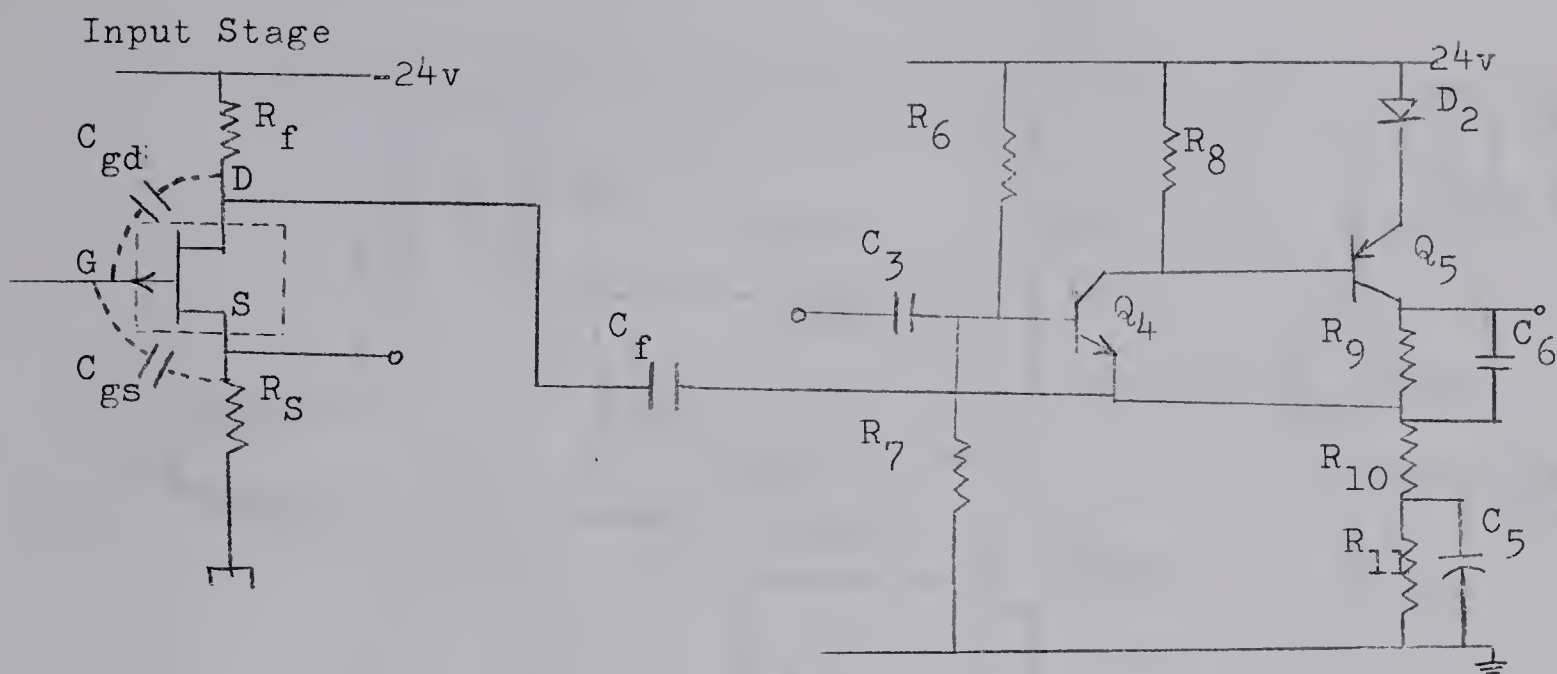
The second stage has a convenient unity gain point at "C" (see Figure 3-9) which may be used to bootstrap the gate-drain capacity of the first stage. This neutralization is accomplished by adding a resistor R_f in the drain lead of the compound F.E.T. and a feedback capacitor C_f between the drain and the unity gain point of the second stage. (Figure 3-8)

The effective C_{gd} is reduced to $C_{gd}/(1 - A_{v1}A_{vC})$ where (15)

A_{v1} is the voltage gain of the compound F.E.T. stage and A_{vC} is as in equation (3.14). The value of R_f is chosen by consideration of the loss in available voltage due to R_f . A value of $R_f = 1.5K$ reduces the available voltage across the compound F.E.T. by 1.5 volts. This has no detrimental effects and as such it is not necessary to reduce R_S . The value of C_f is selected to give an adequately low cut-off frequency with R_f .

$C_f = 0.033$ mfd.

The second stage and feedback configuration is shown in figure 3-8.



$$R_6 = 1.5 \text{ megohms}$$

$$R_{10} = 120 \text{ ohms}$$

$$Q_5 = 2N1305$$

$$R_7 = 2.7 \text{ megohms}$$

$$R_{11} = 15 \text{ K}$$

$$C_3 = 1500 \text{ pf}$$

$$R_8 = 6.8 \text{ K}$$

$$D_2 = 1N456$$

$$C_{f'} = 0.033 \text{ mf}$$

$$R_9 = 1.5 \text{ K}$$

$$Q_4 = 2N3707$$

$$C_5 = 3.3 \text{ mf}$$

Figure 3-8 Second Stage and Gate-Drain Capacity Neutralization

3.3 Third Stage and Final Circuit Configuration

The third stage is similar in design to the second stage and has a gain large enough to give a total system gain of greater than 40db. Referring to the circuit diagram of the complete amplifier (Figure 3-9), the currents through Q_6 and Q_7 were set at 1ma and 10ma respectively. C_8 and C_{10} were chosen to give a lower corner frequency of about 200 cps. C_7 controls the upper frequency response.

Finally transistors Q_3 and Q_8 were added to provide low impedance outputs.

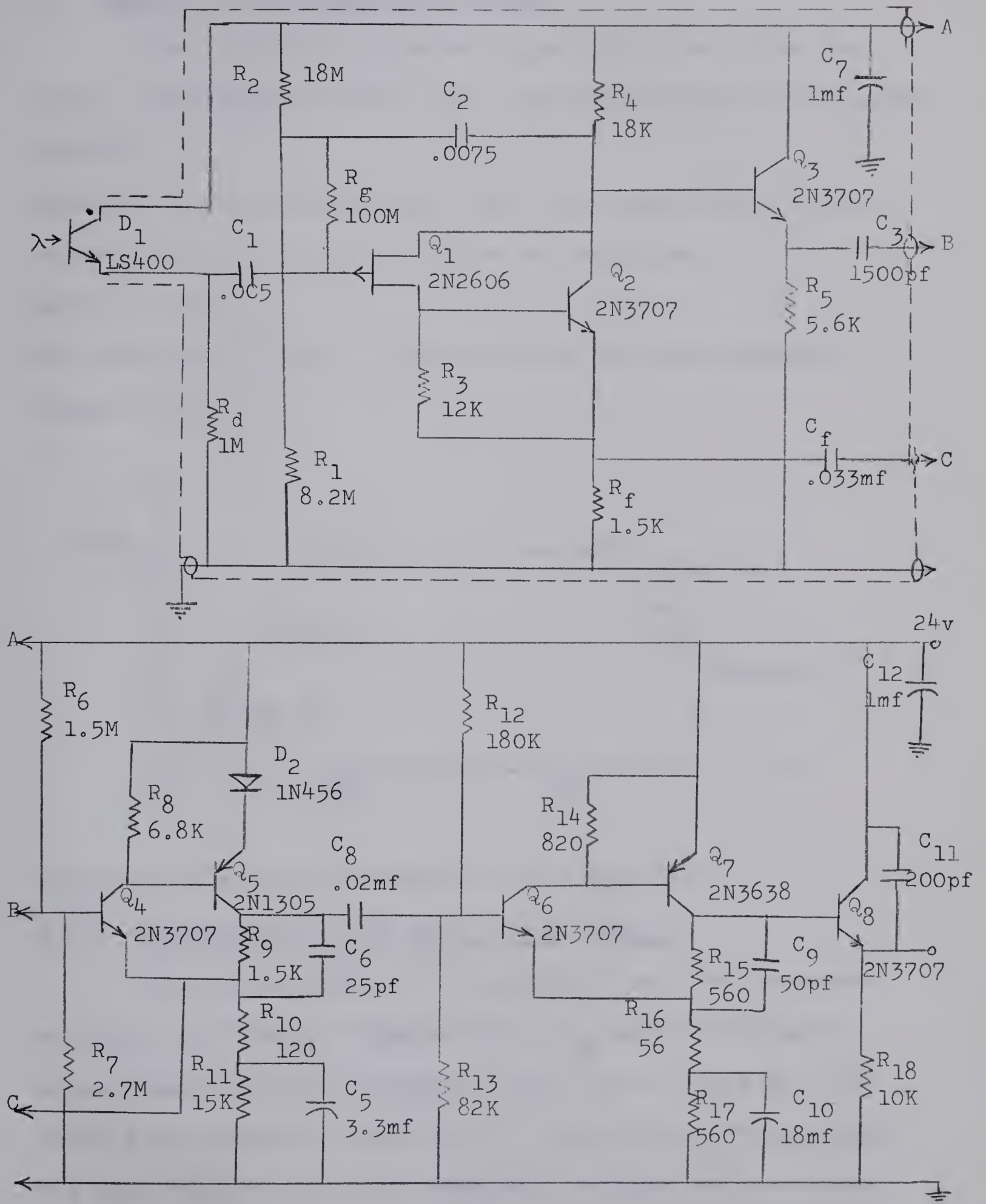


Figure 3-9 Complete Amplifier Circuit Diagram

3.4 Summary of the Amplifier Testing

The electrical characteristics of the amplifier fed from a low impedance source were investigated with the following results:

Rise time = 0.3 microseconds. (The test signal was a 4 micro-second square wave pulse of 0.2 volts amplitude.)

Gain = 42 db

The frequency response of the amplifier was also measured.

(Figure 3-10)

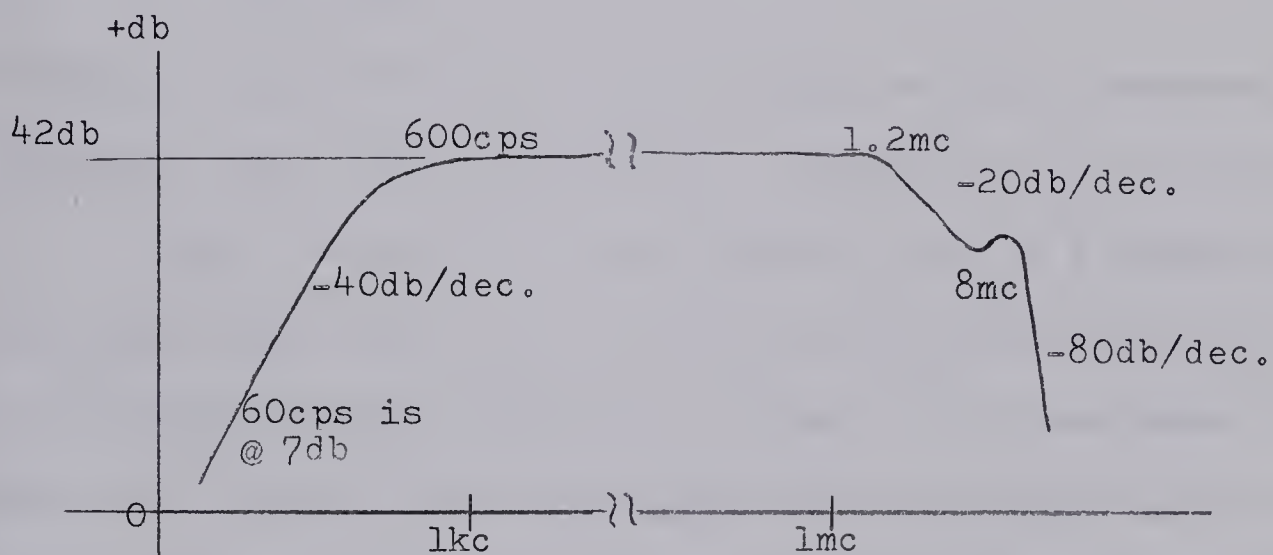


Figure 3-10 Frequency Response of the Amplifier

3.4.1 Measurement of the Input Shunt Capacity

The voltage gain of the amplifier was first measured with C_{in} very large. (Figure 3-11) C_{in} was then reduced, using a small variable capacitor, until the voltage gain at midband had dropped to one-half its value with C_{in} very large. The gain drop is due to the capacitor voltage divider formed between C_{in} and C_S .

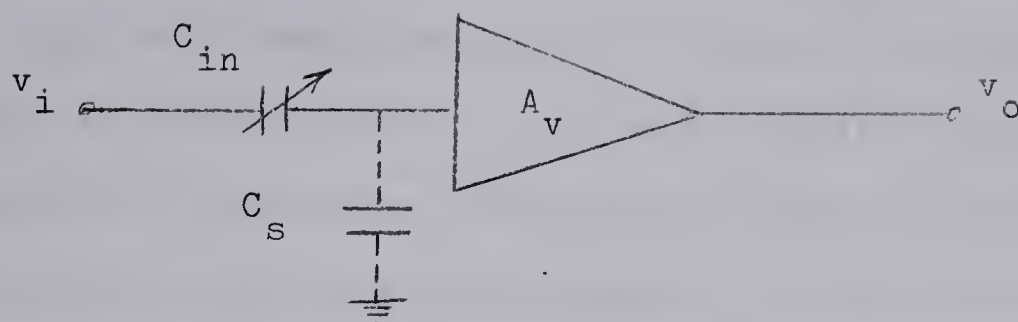


Figure 3-11 Measurement of the Shunt Capacity C_s

Therefore:

$$\frac{C_{in}}{C_{in} + C_s} = \frac{1}{2} \quad \text{and} \quad C_{in} = C_s$$

The value of the variable capacitor C_{in} was then measured on a LC meter and found to be 0.8 pf. Therefore, $C_s = 0.8$ pf.

Since the amplifier will be used with a 1 megohm source resistance (R_d) this value of shunt capacity will further limit the rise time of the amplifier to about $1\frac{1}{4}$ microseconds.⁽³⁾

Since it is anticipated that light pulses as short as 4 microseconds duration will need to be detected, the increase in shunt capacity due to the photodiode and its associated connecting wire must be kept within the order of 1 pf if the required rise time of the system is to be met.

3.4.2 Measurement of the Amplifier Noise Factor

The dominant contribution to the noise factor of the amplifier will be the noise factor of the input stage, (Appendix, equation (A.1)). The noise voltage appearing at the amplifier output terminals with a 1 megohm source resistor

R_d was measured using a true RMS voltmeter (bandwidth of 300kc). The voltage so measured was $V_A = 8.9\text{mv}$. The noise voltage which therefore may be thought of as appearing at the input of the amplifier is V'_A , where V'_A is V_A divided by the gain of the amplifier. The noise factor of the amplifier can be expressed as this rms voltage V'_A divided by the rms voltage due to the thermal noise in R_d .⁽¹⁶⁾ The thermal noise voltage, E_n generated in R_d over a 300kc bandwidth can be found from equation (1.5) $E_n = 0.71 \times 10^{-4} \text{ vrms}$.

Therefore:

$$F = \frac{V'_A}{E_n} = 1.1 \pm 0.5$$

The large error term is due to sources of noise not taken into account such as radiated sources such radio and T.V. stations. However, the measured noise factor agrees fairly well with the noise factor calculated in the Appendix.

CHAPTER 4

System Mechanical Design

4.1 Mechanical Requirements

1) The system must be compatible with the micro-particle charger i.e. it must be easily interchangeable with the photomultiplier tube and be vacuum tight.

2) Placement of the photodiode and associated optics for maximum sensitivity.

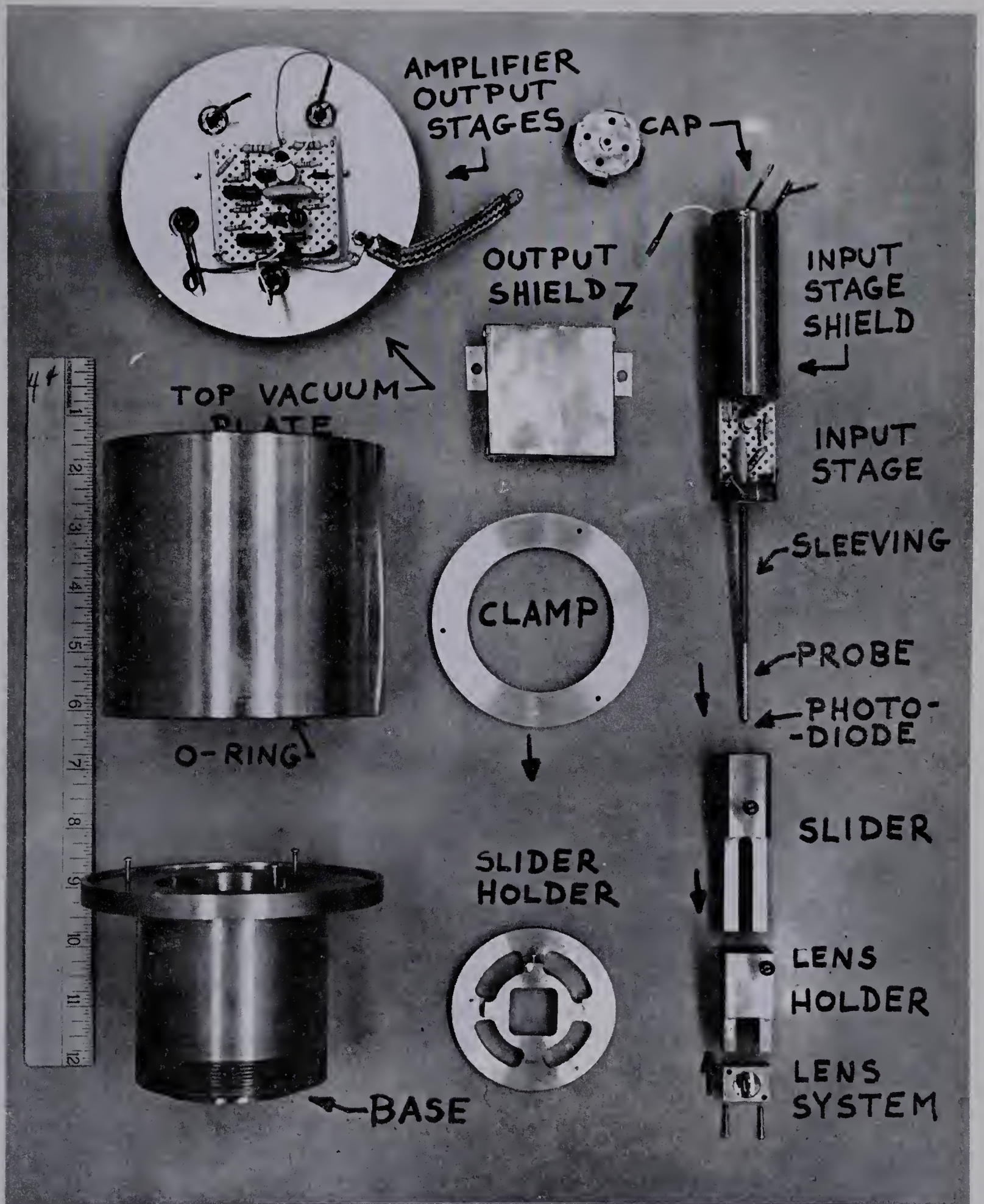
3) Leakage capacity from the signal leads to ground must be kept low.

4.2 System Compatibility

The mechanical details of the micro-particle charger are such as to place certain restrictions upon the physical construction of the solid state detection system. The system must be designed so it can be used in place of the photomultiplier tube with no radical changes in the micro-particle charger. This is accomplished by having the entire solid state detection system (exclusive of the power supply) screw into the same mounting base which is used for the photomultiplier tube. (See photograph 4-2). When the solid state detection system is seated on a rubber O-ring in this mounting base, the entire apparatus is vacuum tight.

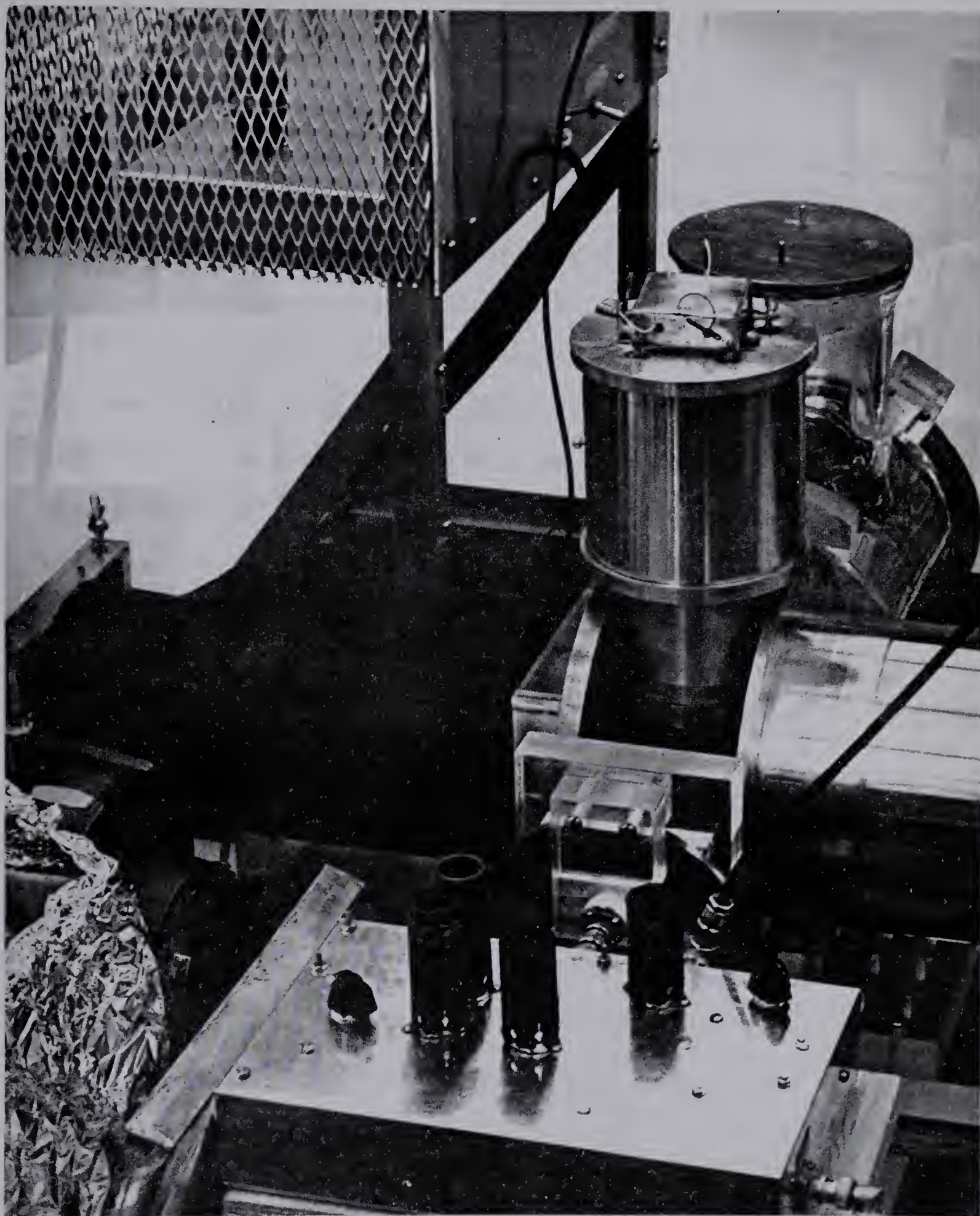
4.3 Optical System and Placement

As discussed in section 1.4.1 it was found that the photodiode must be optically assisted in order to detect the light



Photograph 4-1. Disassembled Photodiode Detector





Photograph 4-2. Complete System

pulses reflected. The collecting lens should be as close to the particle path as is physically possible in order to increase the light pulse pick-up. Due to a light baffle, necessary for photomultiplier operation, the nearest that the collecting lens can approach the particle path is 12 mm. (Figure 4-3).

The diameter of the collecting lens should be as large as possible (equation 1.11). However, since the lens must pass through an opening of 15 x 32 mm., in order to reach within 12 mm. of the particle path, the diameter of the collecting lens is limited to less than 15mm. (Figure 4-3)

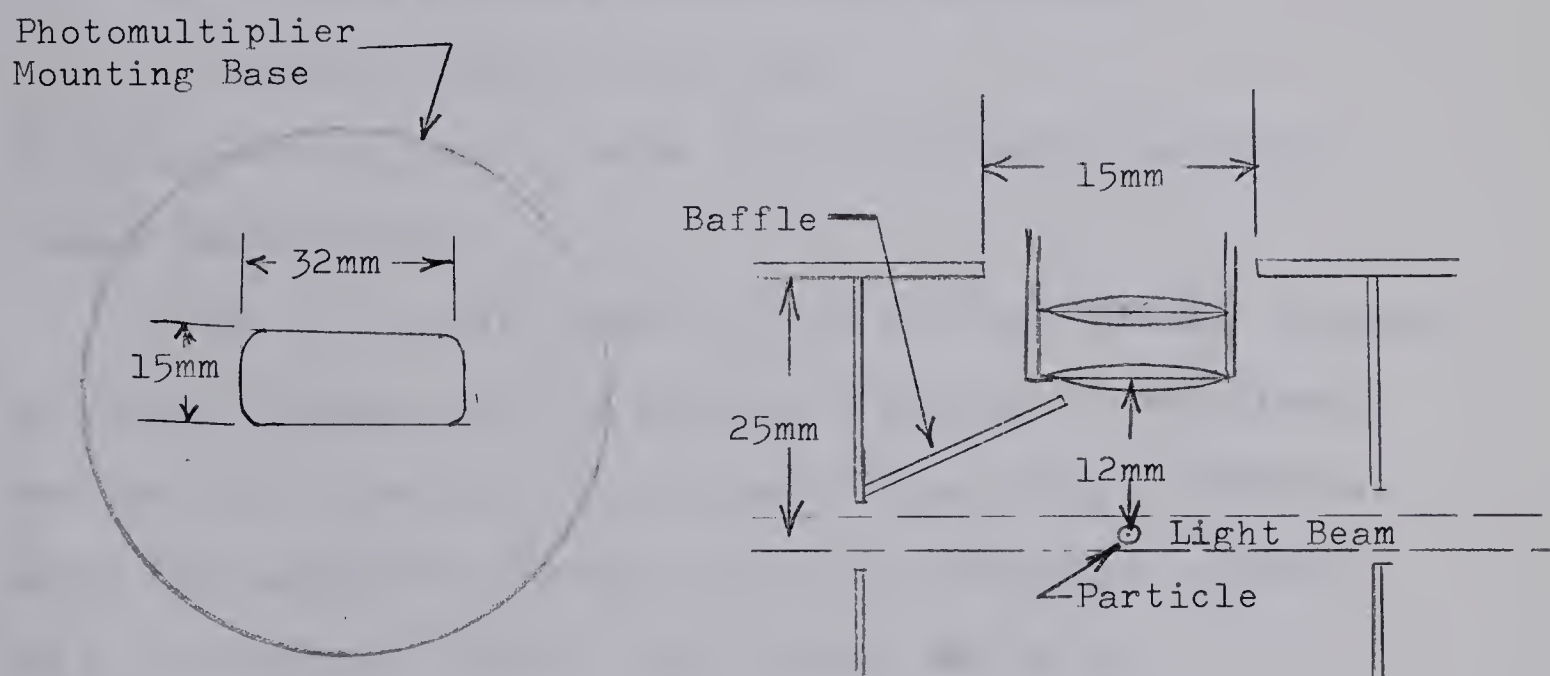


Figure 4-3 Accessibility to the Particle Path

4.3.1 Optical Assistance System

The purpose of the optical system is to increase the effective light intercepting area of the photodiode. This is accomplished by using two lenses in a condenser type arrangement as shown in figure 4-4.

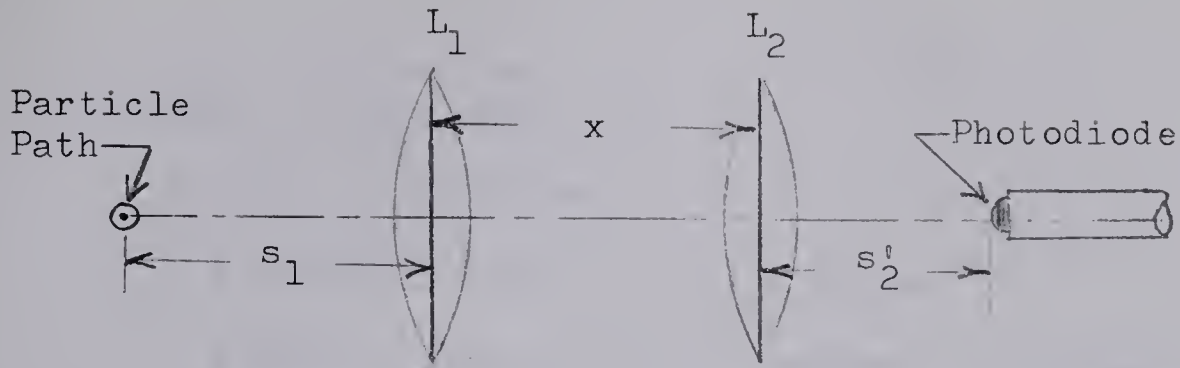


Figure 4-4 Condenser Lens

The above lens system may be calculated by using the lens formula $\frac{1}{s} + \frac{1}{s'} = \frac{1}{f}$ (17) (4.1)

and where light is assumed traveling from left to right:

s = object distance to the left of vertex

s' = image distance to the right of vertex

f = focal length of the lens

In figure 4-4, L_1 and L_2 refer to the collecting and focal lenses respectively.

For L_1 a focal length $f_1 = 29$ mm. was chosen. Assuming an object distance for the collecting lens of 12 mm. (from section 4.3), equation (4-1) gives a value of $s_1' = -20.4$ mm. where the subscript 1 refers to L_1 i.e. the image projected by L_1 is imaginary and 20.4 mm. to the left of L_1 .

The object distance of L_2 is:

$$s_2 = s_1' + x$$

Where x is the distance between the lenses = 5 mm.

Thus $s_2 = 25.4$ mm.

In order for the light signal to be concentrated on the photodiode the image distance s_2' of L_2 must be positive (to the right of L_2). This implies that the focal length f_2

of L_2 must be less than s_2 .

Thus $f_2 < 25.4$ mm.

A suitable choice is $f_2 = 12$ mm.

Substituting into (4.1) results in a final image distance of 23 mm. to the right of L_2 . This is where the photodiode should be placed.

The lenses chosen were:

L_1 with a 11.5 mm diameter and a 29 mm focal length.

L_2 with a 11.5 mm diameter and 12 mm focal length.

All the above calculations are on the assumption that infinitely thin lenses are used. Since the actual lenses do have an appreciable thickness the above image distances can only be considered approximate. To correct for any inaccuracies, and for ease in setting up the final system, both the object distance s_1 and the distance the photodiode is placed from L_2 are adjustable. The adjustments are accomplished by means of a telescoping slider which contains the condenser lens system and a copper tube probe which contains the photodiode. Photograph 4-1 illustrates the disassembled lens holder, slider and probe.

4.4 Signal to Ground Capacity Shielding

The location of the particle path makes it necessary to run the signal lead from the photodiode a distance of over three inches to the input stage of the amplifier. This signal lead is in close proximity to chassis ground during most of this

run. In order to keep the signal to ground capacity within bounds, both the signal lead from the photodiode and the input stage must be guarded from ground. The guarding is accomplished by holding the copper-tube probe enclosing the photodiode and signal leads at the signal potential. The input stage is mounted directly at the end of the probe, inside the vacuum, and is completely enclosed inside a light copper pipe held at the same guard potential. Thus most of the signal to ground capacity is eliminated.

The method of shielding is illustrated in photograph 4-1. The sleeving on the bootstrapped copper-tube probe isolates the probe from the chassis ground.

The guard potential obtained from the unity gain point C in figure 3-9 and 4-5. Thus this bootstrapping transfers the input shunt capacity to the output of the unity gain stage where low impedance levels make it insignificant.

The remaining stages of amplification are mounted outside the vacuum system upon the top vacuum plate (photograph 4-1 and 4-2). Connection is made to the input stage by means of vacuum tight electrical feed-throughs attached to clip leads.

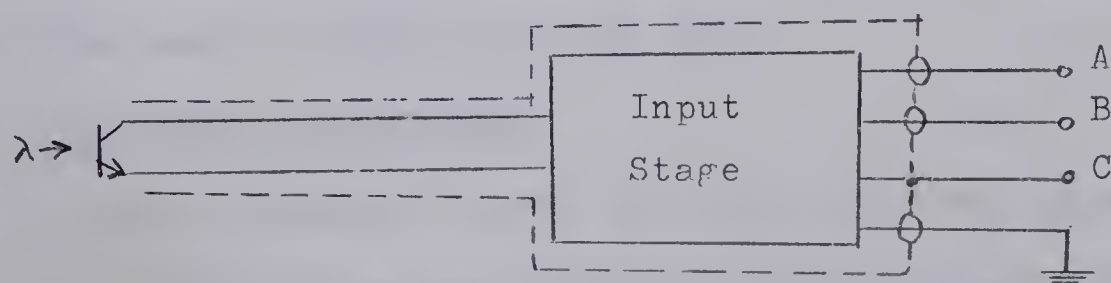


Figure 4-5 Bootstrapped Guarding of the Input

CHAPTER 5

Summary of System Testing

5.1 System Rise Time Measurement

The photodiode optical detection system was first tested outside the micro-particle accelerator to determine if the required system rise time response had been obtained.

The test signal consisted of very weak light pulses from a stobo-tach (rise time of 0.5 microseconds). A darkened room was used to simulate the low ambient light levels expected in the micro-particle charger. The intensity of the light pulse reaching the collecting lens was adjusted by increasing the distance between the light pulse source and the photodiode detection system (distances in the order of 20 feet were used) and covering the stobo-tach with layers of cloth until pulse output of about 0.2 volts peak was observed at the amplifier output terminals.

It was found that the rise time of the system remained fairly constant over a wide range of signal to noise ratios. The rise times so measured fell in the range of 3.5 to 4 microseconds. This showed that the shunt capacity of the photodiode detection system had been sufficiently reduced to enable the rise time design criterion to be met.

5.2 Delay Time Measurement

The arrangement shown in figure 5-1 was used to measure the delay time of the photodiode detection system. The delay

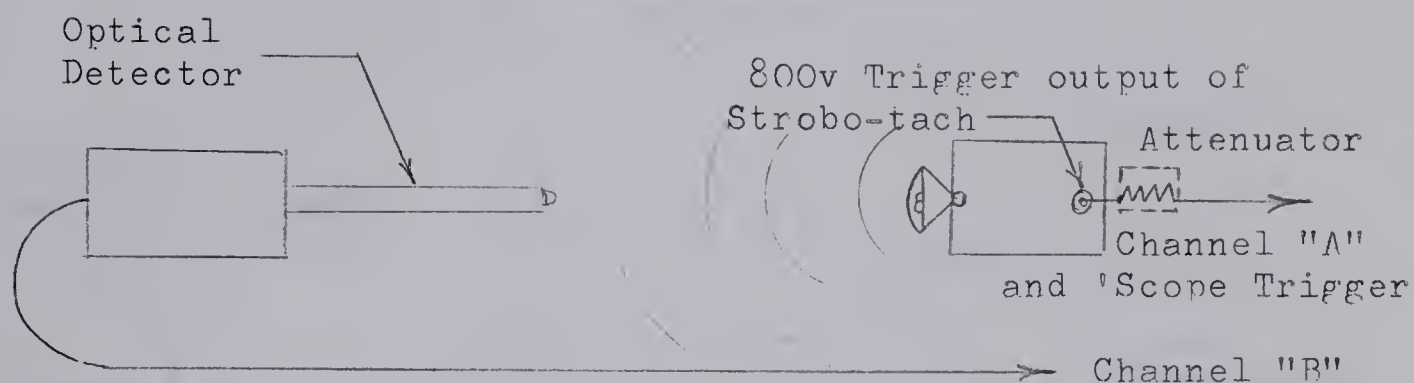


Figure 5-1 Measurement of the System's Delay Time

time between when the strobo-tach is triggered to when a pulse output was measured. The delay time so found was 0.2 microseconds. Part of this delay time also includes the time between when the stro-tach is triggered to when a light pulse appears. However, the delay time is insignificant as the micro-particle will have traversed less than 0.1 mm in this time.

5.3 Displaying of Output Signals

The outputs from the solid state detector and a charge sensitive amplifier were displayed on two beams of a delayed triggered, high retention oscilloscope. The charge sensitive amplifier detected the micro-particles before and after they entered the space containing the light beam. The oscilloscope was triggered by the output of the charge sensitive amplifier whenever a particle passed through the charge detector 1. (Figure 5-2). To enable a faster sweep to be used with the solid state detector output the triggering of channel A was delayed from channel B. The delay was set as the estimated time it takes the particle to travel from the charge detector 1

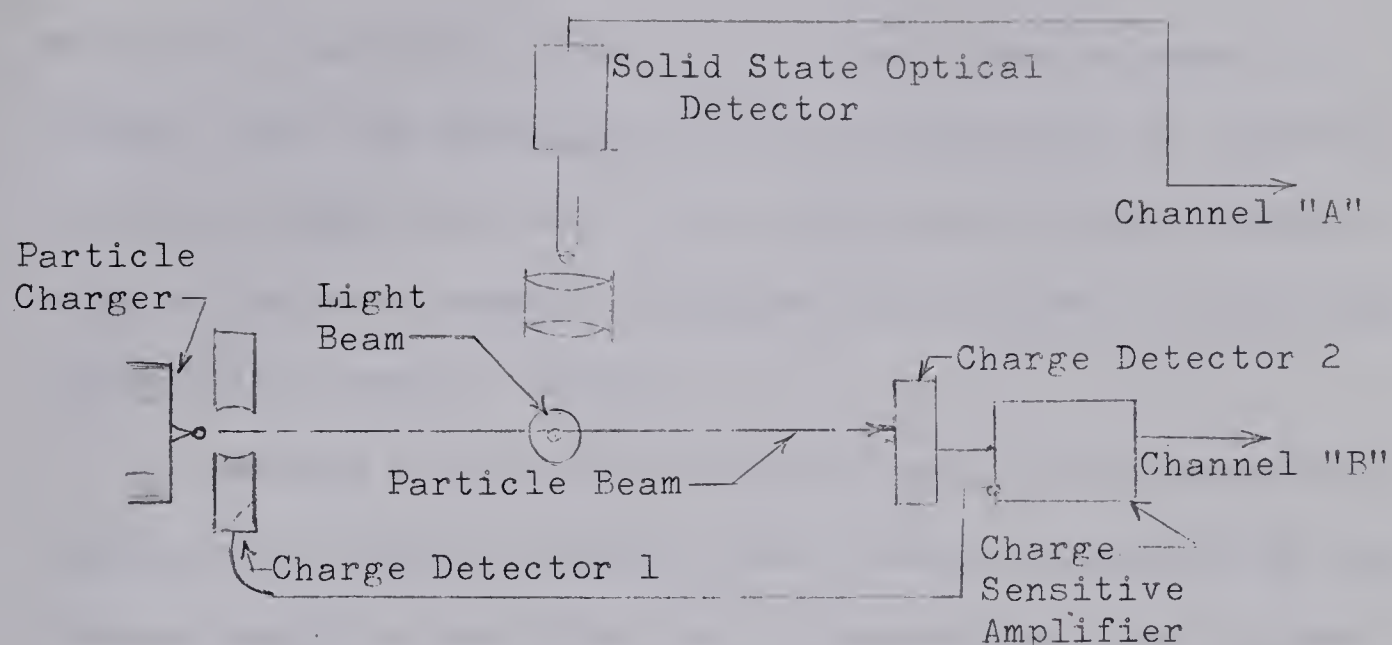


Figure 5-2 Method of Displaying the Outputs

to the light beam. Charge detector 2 confirms if the particle actually passed through the light beam.

5-4 Summary of the Testing and Results of the Solid State Optical Detection System When Used with the Micro-Particle Charger

Initially the optical system of the solid state detector was adjusted by inserting a 2.4 mm diameter steel rod along the axis of the particle beam (Figure 5-3). The light scattered from this rod had enough 60 cps component to be observed at the output of the solid state detector amplifier.

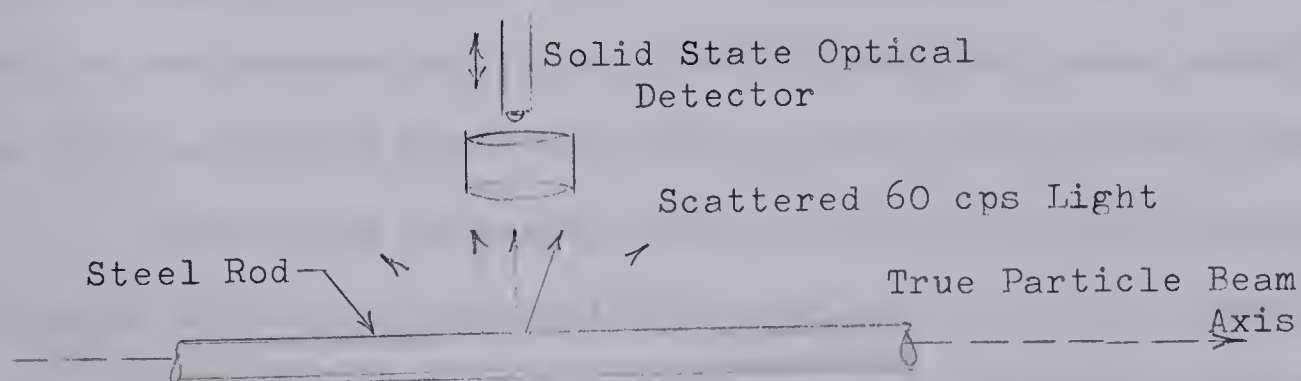


Figure 5-3 Apparatus for Optical Adjustment

With the lens set as close to the light beam as possible (Figure 4-3) the photodiode probe was adjusted for maximum scattered light pick up. This adjustment was very critical with a 2 mm misalignment resulting in an order of magnitude drop in the observed output.

During the course of the following two experiments, during which several hundred particles were detected by the charge sensitive amplifier, no corresponding signal pulses were observed from the solid state optical detector. As it had been previously observed that the adjustment of the optical system was extremely critical, it was decided to realign the optical system by focussing it on the light scattered from a rod of 1.3 mm diameter positioned along the particle beam axis as before. (See figure 5-3) With this adjustment the solid state detection system was made more sensitive to particles travelling very near the true axis of the particle beam. Previously the solid state optical detection system was more sensitive to particles travelling near the edge of the particle beam. With the new adjustment it was observed that the detection system was nearly an order of magnitude more sensitive to light scattered near the center of the particle beam axis.

During the following test more than 500 particles were detected by the charge sensitive amplifier. Of these more than 50 passed through the focus of the light beam as was indicated by their interception by the second charge sensitive detector. (Figure 5-2)

In three cases extremely large signals were observed from the charge sensitive amplifier and at the same time signal output pulses were observed from the solid state optical detector. The amplitude of these pulses was unexpectedly large on both the charge sensitive amplifier and the solid state optical detector traces. Therefore both traces went partially off scale and no positive correlation between the two pulses could be established.

It is therefore indicated that the optical detection of the micro-particles using a photodiode is not feasible with the present system. Thus even though there is an indication that the solid state optical detector responds to very large particles, the frequency of occurrence of these large particles is so low that it is experimentally unfeasible to positively identify and record these pulses without major alterations in both the charging and solid state detection systems.

The following factors could account for the lack of general particle detection:

- 1) Reflectivity of the micro-particles could be considerably below the assumed reflectivity factor of 0.50. The reflectivity could be as low as 1%. This low reflectivity is also indicated by recent tests with a photomultiplier optical detector where output signals were as low as two orders of magnitude below that expected.

2) Low usable power in the light beam.

Although the concentrated arc light power in the 2mm beam is 100 mw the actual light power in the wavelengths to which the photodiode is most sensitive could be much less.

Recommendations

Using the experience gained from this project a solid state optical detection system of much greater sensitivity could be designed. It is recommended that in such a system use be made of solely solid state devices including the light source.

Recent developements in semiconductor light sources has resulted in an efficient device which will put 50 milliwatts of light power into a 90° cone. The light frequency versus the output light power of this light source peaks in the same frequency range as the photodiode's light frequency versus sensitivity curve. The solid state light source can be heat sunk and mounted inside the vacuum. Its small physical size would also enable it to be placed very close to the particle beam, thus eliminating the need for a concentrating lens system. The photodiode lens system could also be placed very close to the particle path at right angles to the light source. The very small distances involved would result in greatly improved light signal pick up over the present system.

Bibliography

- 1) Hulst, H.C. van de: "Light Scattering by Small Particles" Toronto, Wiley, 1957, Section 4-2.
- 2) Philips Electron Tube Division: "Photomultipliers for Scintillation Counting", 20/763/D/E-6-'59.
- 3) Miller, J.R. (ed.): "Texas Instrument's Communications Handbook, Part 2", Texas Instrument's handbook series, 1965.
- 4) Walston, J.A. (ed.): "Transistor Circuit Design", Texas Instruments Inc., Toronto, McGraw Hill, 1963, Appendix pages 509-513.
- 5) I.R.E. Committee: "Representation of Noise in Linear Two Ports", Proc. I.R.E., 1960, page 73.
- 6) Terman, F.E.: "Electronic and Radio Engineering", Fourth Edition, Toronto, McGraw Hill, 1955, Section 9-1.
- 7) Siliconix Corporated Application Note: "High Input Impedance UNIFET Amplifiers", Feb. 1963.
- 8) Siliconix Corporated Application Note: "Low Pinch-Off Voltage F.E.T.'s", May, 1963
- 9) Sevin, L.J.: "Field Effect Transistors", Toronto, McGraw Hill, 1965, Section 2-2.
- 10) Siliconix Corporated Application Tip: "Measurement of I_{GSS} ", Nov. 27, 1963.
- 11) Sevin, L.J.: "Field Effect Transistors", Toronto, McGraw Hill, 1965, page 56.
- 12) Edwards, E.M.: "A D.C. Amplifier and Reference Voltage Supply Suitable for Use in a Magnetic Current Regulator", M.Sc. Thesis, University of British Columbia, 1964.
- 13) Edwards, E.M.: "Bootstrapped Bias Analysis", Presented at the Canadian Electronics Conference, Toronto, November, 1965 (unpublished)

- 14) Walston, J.A.: "Transistor Circuit Design", Texas Instruments Inc., Toronto, McGraw Hill, 1963, Page 253.
- 15) Sevin, L.J.: "Field Effect Transistors", Toronto, McGraw Hill, page 67.
- 16) Nielson, E.G.: "Behavior of Noise Figure in Junction Transistors", Proc. I.R.E., 1957, page 958.
- 17) Jenkins, F.A., White, H.E.: "Fundamentals of Optics", Toronto, McGraw Hill, 1957, Section 4-40.
- 18) Tucker, R.L.: "Biological Field Effect Transistor Amplifier", M.Sc. Thesis, University of Alberta, Electrical Engineering Dept., 1965, Appendix 2.
- 19) Blaser, L.: "The Design of Low Noise, High Input Impedance Amplifier", Fairchild Application Data, APP-36, 1961.
- 20) I.R.E. Committee: "Standards on Measuring Noise in Linear Two Ports", Proc. I.R.E., 1960, page 61.

APPENDIX

Noise Factor

A.1 To find the noise factor of the compound F.E.T. of the input stage, the open loop equivalent of the compound will be studied (figure A-1). This can be done since the addition of feedback will not effect the noise factor of the amplifier i.e. the signal to noise ratio will remain the same.

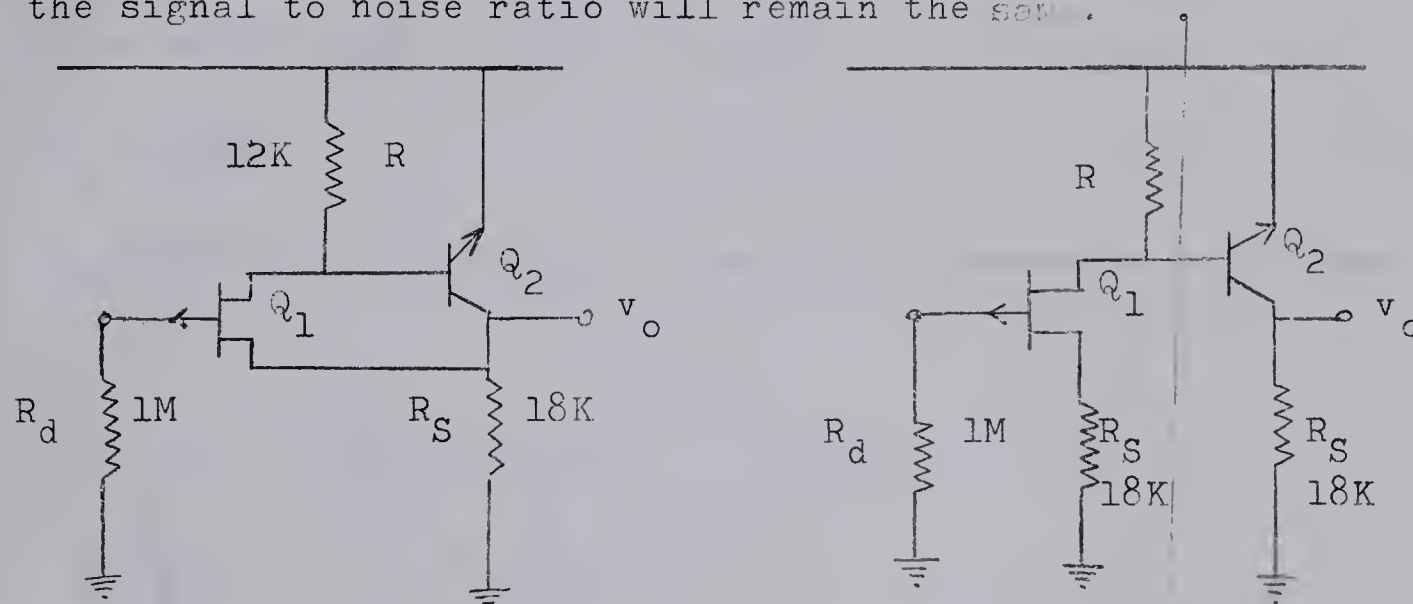


Figure A-1 Open loop equivalent of the hybrid compound F.E.T.

The open loop equivalent can be regarded as two cascaded amplifiers with noise factors of F_1 and F_2 , and power gains of G_1 and G_2 . The subscript 1 refers to the F.E.T., Q_1 , amplifier and the subscript 2 refers to the silicon transistor, Q_2 , amplifier (figure A-2).

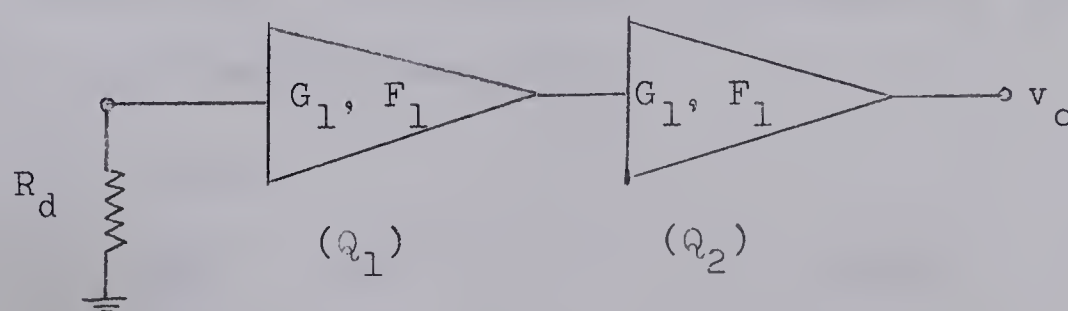


Figure A-2 Cascaded amplifiers

The noise factor of the amplifier cascade of figure A-2 is: (20)

$$F = F_1 + \frac{F_2 - 1}{G_1} \quad (A.1)$$

Where: $\frac{\text{Available noise power output}}{\text{Available noise power output due to thermal noise in } R_g} = \frac{P_A}{P_g}$ (9)

And:

$$P_A = 4kTB + R_d i_n^2 + e_n^2 / R_d + 2e_n i_n \gamma \quad (A-2)$$

$$P_g = 4kTB$$

R_d = internal resistance of the signal generator = 10^6 ohms

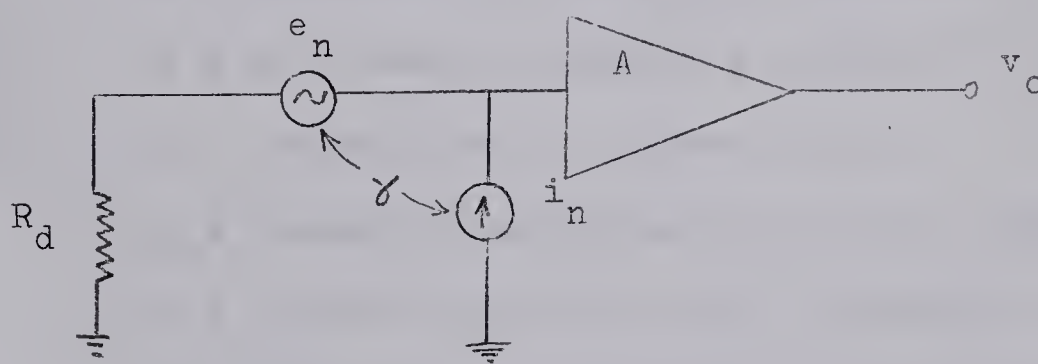


Figure A-3 Noise signal to the amplifier

i_n and e_n represent the noise signal generated in the amplifier A and placed outside the amplifier.

A-2 Calculation of F_1

In an F.E.T. the correlation coefficient, γ , between i_n and e_n is approximately zero and ()

$$i_n^2 = 2qI_{GSX}B$$

$$e_n^2 = \frac{4kT(1 + \frac{f_{cl}}{f})}{g_m} df \quad (A.3)$$

Therefore:

$$e_n^2 = \frac{4kT}{g_m} \left(B + \int_{f_1}^{f_2} \frac{f_{cl}}{f} df \right)$$

$$e_n^2 = \frac{4kT}{g_m} \left(B + f_{cl} \ln \frac{f_2}{f_1} \right) \quad (A-4)$$

Where:

q = electron charge = 1.6×10^{-19} coulomb

I_{GSX} = gate source leakage current at operating conditions
of Q_1

B = bandwidth of the F.E.T. amplifier = 2×10^6 cps

k = Boltzmann's constant = 1.37×10^{-23} joules/ $^{\circ}K$

T = temperature in degrees Kelvin

g_m = forward transconductance of Q_1 = 200×10^{-6} mhos

f_{cl} = flicker noise turn over frequency of $Q_1 \approx 1$ kc.

f_1 = lower corner frequency of the closed loop amplifier = 1 cps

f_2 = upper corner frequency of the closed loop amplifier
= 2×10^6 cps

Substituting equations (A.3) and (A.4) into equation
(A.2) gives the equivalent noise power input to the F.E.T.
amplifier:

$$P_{A_1} = 4kTB + 2qI_{GSX}BR_d + \frac{4kT}{g_m R_d} \left(B + f_{cl} \ln \frac{f_2}{f_1} \right) \quad (A.5)$$

Since: $F_1 = \frac{P_{A_1}}{P_g}$, F_1 can be calculated:

$$\underline{F_1 = 1.03}$$

A.2.1 Calculation of G_1

(20)

The power gain G_1 can be expressed as

$$\frac{v_{o1}^2}{R_L} \bigg/ \frac{v_i^2}{R_d} = A_v^2 R_d / R_L$$

Where $A_{v1} \approx \frac{R_L' g_{fs}}{1 + R_L' g_{fs}}$

where $R_L' = R // (h_{ib2}, h_{fe2})$

$$A_{v1} \approx 0.24$$

Therefore $G_1 \approx 48$

A.3 Calculation of F_2

The noise factor F_2 of the silicon transistor stage may be expressed as: (19)

$$F_2 = F_o + \frac{R_n}{R_o} \left(\sqrt{\frac{R_g}{R_o}} - \sqrt{\frac{R_o}{R_g}} \right)^2 \quad (A.6)$$

Where:

$$F_o \approx 1 + \frac{1}{h_{fe2}}$$

$$R_o \approx \sqrt{h_{fe2}} h_{ib2}$$

$$R_n \approx \frac{h_{ib2}}{2}$$

$$R_g \approx R = 12K$$

Substituting the mixed h parameters of Q_1 into equation (A.6)

gives:

$$F_2 = 1.58$$

Therefore from equation (A.1) the hybrid compound F.E.T. input stage has a theoretical noise figure of $F \approx 1.04$

B29844